PALAIOS
Emphasizing the impact of life on Earth's history

PALAIOS, 2017, v. 32, 135–152
Research Article
DOI: http://dx.doi.org/10.2110/palo.2016.039

TAPHONOMIC CLOCK AND BATHYMETRIC DEPENDENCE OF CEPHALOPOD PRESERVATION IN BATHYAL, SEDIMENT-STARVED ENVIRONMENTS

ADAM TOMAŠOVÝCH,[1] JÁN SCHLÖGL,[2] ADRIÁN BIROŇ,[3] NATÁLIA HUDÁČKOVÁ,[2] AND TOMÁŠ MIKUŠ[3]
[1]*Earth Science Institute, Slovak Academy of Sciences, Dúbravská cesta 9, 84005, Bratislava, Slovakia*
[2]*Department of Geology and Paleontology, Comenius University, Mlynska dolina, Ilkovičova 6, 84215, Bratislava, Slovakia*
[3]*Earth Science Institute, Slovak Academy of Sciences, Ďumbierska 1, 97401, Banská Bystrica, Slovakia*
email: geoltoma@savba.sk

ABSTRACT: **The dependence of skeletal alteration on time spent in the taphonomic active zone (TAZ) can generate a taphonomic clock, which can be used to quantify scales of time averaging and rates of skeletal production and recycling in the fossil record. However, the strength of the taphonomic clock is variable in present-day shallow marine environments and it is unclear how this strength varies with depth. Here, we assess the strength of the taphonomic clock in *Nautilus macromphalus* dead shells that were collected in cool-water, sediment-starved, epi- and mesobathyal environments off New Caledonia and range in postmortem age from few decades to several millennia. We find that, first, differences in the onset and extent of alteration states in the epibathyal zone (< 750 m) segregate well-preserved shells with red stripes (less than ~ 200 years) from encrusted shells with faded colors and extensively bored by sponges (~ 400 years), and from strongly fragmented, bored, and coated shell relicts (> 1,000 years). The onset of dissolution and formation of clay-goethitic coating occurs earlier (~ 200 years) in the mesobathyal zone (> 750 m) than in the epibathyal zone. Clay-goethitic rims and boring infills show signs of microbial binding, pelletization, and coccolith dissolution and can represent nascent stages of glauconitization. Second, shells several centuries old show differences between right and left flanks (1) in the degree of encrustation and sponge bioerosion in the epibathyal zone and (2) in the extent of clay-goethitic coating in the mesobathyal zone. The upper flanks are ultimately removed in both depth zones, leaving relict half-shells that are millennia old. Third, the depth dependence of alteration can reflect a bathymetric decline in disintegration rates by heterotrophic borers due to a reduced productivity in the mesobathyal zone and an increase in dissolution rates due to the proximity of the aragonite compensation depth. The between-flank asymmetry in preservation implies (1) horizontal position of shells close to the sediment-water interface for several decades or centuries without being overturned or subjected to reworking and (2) shell exposure to two distinct taphonomic regimes separated by few centimeters, with the upper flank located in the TAZ and the lower flank facing a less aggressive sediment zone. The stable exposure of shells in the taphonomic active zone and slow alteration rates in bathyal environments allow discriminating between within-habitat time-averaged assemblages on one hand and environmentally or stratigraphically condensed assemblages on the other hand.**

INTRODUCTION

Estimating time averaging in the fossil record is of high importance because the temporal resolution significantly affects taxonomic and ecological structure of ecological communities and metacommunities (Tomašových and Kidwell 2010; Kidwell 2013; Miller et al. 2014; Terry and Novak 2015). Several criteria allow identification of scales of time averaging in fossil assemblages on the basis of paleoecological, sedimentological, taphonomic (Fürsich 1978; Kidwell 1989; Zuschin and Stanton 2002; Bennington 2003), sequence stratigraphic (Scarponi et al. 2013), geochronological (Weedon et al. 1999), and geochemical evidence (Goodwin et al. 2004; Nieto et al. 2008; Benito and Reolid 2012). Such criteria can discriminate among (1) rapidly buried census assemblages (< 1–10 years); (2) assemblages averaged within a single habitat (~ 10–1,000 years); (3) environmentally condensed assemblages averaged across multiple habitats (~ 1,000–100,000 years); and (4) biostratigraphically condensed assemblages (> 100,000–1 Myr years or more) (Kidwell 1998). However, the last three categories span a very broad range of temporal durations, which can also vary among environments and among ecosystems with different rates of spatial or temporal turnover in species composition (Tomašových and Kidwell 2010). Therefore, the duration of time averaging is difficult to constrain in fossil assemblages (Kowalewski and Bambach 2003). One of these criteria is represented by a so-called taphonomic clock (Kidwell 1993): as dead shells are exposed in the taphonomic active zone (TAZ) in the mixed layer, they tend to accrue more skeletal alteration with increasing postmortem age (Pilkey et al. 1979; Norris and Grant-Taylor 1989; Powell and Davies 1990; Tomašových et al. 2006). This clock can represent a unique source of information to estimate scales of time averaging and to unmix assemblages into cohorts differing in postmortem age (Belanger 2011; Yanes 2012; Albano 2014; Hassan et al. 2014).

However, inferring the degree of time averaging on the basis of a taphonomic clock is difficult because the relation between alteration state and postmortem age is weak in shallow marine environments (Flessa et al. 1993; Kowalewski et al. 1994; Kidwell et al. 2005; Torres et al. 2013). First, skeletal alteration rates typically decline with sediment depth and/or vary horizontally, and alteration processes thus can be ineffective during a temporary displacement of shells from the TAZ: old shells can show minor skeletal damage when residing in a less aggressive sequestration zone (SZ,

Published Online: March 2017
 0883-1351/17/032-135/$03.00

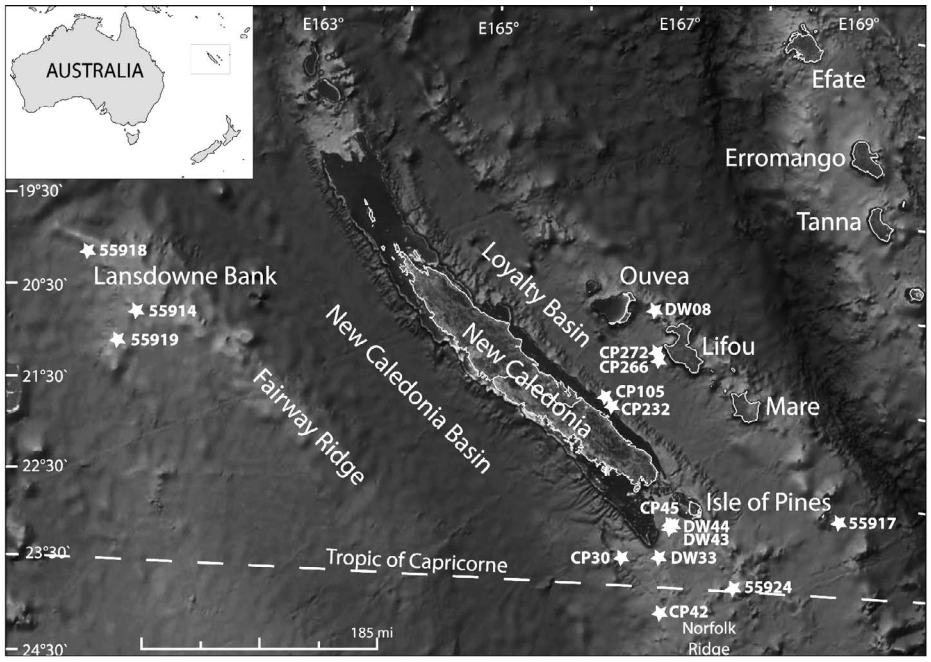

FIG. 1.—Location of stations with dead shells of *Nautilus macromphalus*. Google Earth (Version 7.1.2.2041) [Software]. Mountain View, CA: Google Inc. (2014).

Tomašových et al. 2014) and/or when reworked back to the TAZ (Meldahl et al. 1997; Olszewski 2004). Second, a taphonomic clock will not discriminate between young and old cohorts when alteration processes occur at fast rates and even very young shells are completely altered. Several previous studies thus dismiss the applicability of a taphonomic clock in the fossil record. However, we think that this conclusion is premature, especially because conspicuous alteration tends to be associated with very old skeletal remains (Nelson and Bornhold 1983; Rivers et al. 2007). We suspect that (1) the displacements of shells between the TAZ and the SZ (e.g., via burial and exhumation) that can decouple the positive relation between postmortem age and skeletal alteration do not necessarily apply to all depositional environments and (2) some alteration processes can act at slow rates, such as glauconitization (Baldermann et al. 2013) or growth of ferromanganese crusts (Oda et al. 2011) owing to very low concentrations of K, Fe, or Mn in seawater, and thus can provide minimum postmortem ages even when skeletal particles do not spend all time in the TAZ.

In this study, we (1) quantify the strength of a taphonomic clock and (2) estimate bathymetric dependence of preservation in dead shells of chambered cephalopods (*Nautilus macromphalus*) occurring around New Caledonia in epibathyal (< 750 m) and mesobathyal (> 750 m) environments. Specifically, we test whether variation (1) in alteration of external flank surfaces and (2) in asymmetry in alteration between both flanks can be explained by variation in postmortem age and by variation in water depth. We show that these shells were horizontally exposed with their upper flanks in the TAZ for decades or centuries. We suggest that such conditions generate a relatively strong taphonomic clock and shed light on the conspicuous preservation of cephalopod half-shells (Maeda and Seilacher 1996; Olóriz et al. 2004). Although methodological, statistical, and clade-specific factors affect the strength of the taphonomic clock (Kowalewski et al. 1994; Kidwell et al. 2001), we suggest that targeting death assemblages (1) from environments with stable sea-floor conditions (with sediments not subjected to vigorous mixing) and/or (2) from environments where alteration processes are slow can provide appropriate conditions for the application of the taphonomic clock in the fossil record.

The application of a taphonomic clock to fossil assemblages with chambered cephalopods is paramount because cephalopods are extensively used in stratigraphic (Brühwiler et al. 2010), biogeographic (Brayard et al. 2007), ecologic (Jacobs et al. 1994; Olóriz et al. 2006; Kruta et al. 2014; Naglik et al. 2016), evolutionary (Gerber 2011), and sedimentological inferences (Lukeneder and Mayrhofer 2014). However, most taphonomic studies focused on laboratory experiments (Wani 2004; Wani et al. 2005) and the water-column fate of floating cephalopod shells, inferring their buoyancy and postmortem drift (Reyment 1973; Chirat 2000), depth of implosion (Chamberlain et al. 1981), and accrual of encrustation and bioerosion (Seuss et al. 2015a). In contrast, their fate on the sea-floor under natural conditions remains poorly known (Seilacher et al. 1976; Maeda and Seilacher 1996). Several actualistic studies assessed sea-floor preservation of *Nautilus* in death assemblages from beach and backshore environments (Mapes et al. 2010a, 2010b; Hembree et al. 2014) and submarine caves (Landman et al. 2014), but studies assessing their preservation in deep-water environments within their native habitat are rare (Mapes et al. 2010a; Seuss et al. 2015b). Here, relatively good support for a taphonomic clock allows us to reconstruct preservation pathways affecting dead shells of *Nautilus* exposed on the sea-floor close to its preferred water depths, and to predict postmortem age of chambered cephalopods on the basis of their preservation in comparable environments.

METHODS

Material

Dead shells of *Nautilus macromphalus* were sampled along the southeastern margin of New Caledonia (off Lifou Island, off Isle of Pines, and off Great Southern Reef), at Lansdowne Bank (located between New Caledonia and the Chesterfield Islands), and at the Antigonia Seamount (Fig. 1). A total of 21 specimens were sampled with beam trawls and dredges at eleven sites in 1985 and 1987 in the course of Biocal and Biogeocal campaigns (De Forges 1990) and obtained from the Université de Bourgogne (Table 1). To increase the sample size, five specimens sampled in 2003 and 2005 and described by Mapes et al. (2010a) were obtained from the American Museum of Natural History (New York). The water depth ranges between 330 and 1,663 m, spanning seawater temperatures that decline from 15–16°C at 300 m to 7°C at 700 m water depth in the epibathyal zone, and to 3–5°C at 1,600 m water depth in the mesobathyal zone (Roux et al. 1991; Roux 1994). Twenty-six specimens were age-dated by radiocarbon-calibrated amino acid razemization (AAR)

TABLE 1.—*Water depth, geographic coordinates, sampling year, and postmortem age of 24 specimens, together with alteration scores. Key: M.p.f. = more pristine flank; L.p.f. = less pristine flank; 0 = pristine preservation; 1 = altered.*

Specimen ID	Water depth (m)	Sampling year	Latitude	Longitude	Postmortem age (years)	Lower 95% confidence interval on age	Upper 95% confidence interval on age	Less pristine flank	Body chamber completeness	M.p.f.-phragmocone completeness	M.p.f.-sheen loss
CP105	332.5	1985	-21.5118	166.362	245	110	620	right	0	0	1
CP42/1	380	1985	-23.7523	167.202	97	20	360	left	0	0	1
55924	383	2003	-23.3812	168.0143	19	19	19	right	0	0	0
DW43	400	1985	-22.7702	167.2417	581	320	1190	left	0.5	0.5	1
55914	418	2005	-20.7988	161.0035	286	150	690	right	0	0.5	1
CP45/1	430	1985	-22.789	167.2467	358	180	810	right	0.5	0	1
CP45/2	430	1985	-22.789	167.2467	169	80	280	left	1	0.5	1
CP45/3	430	1985	-22.789	167.2467	416	220	930	left	0.5	0.5	1
CP45/4	430	1985	-22.789	167.2467	122	50	430	right	0.5	0	0
DW08	435	1985	-20.5725	166.8983	280	150	710	right	0.5	0.5	1
DW44/1	445	1985	-22.7883	167.2383	324	160	760	left	0.5	0	1
DW44/2	445	1985	-22.7883	167.2383	173	70	510	left	0.5	0.5	1
DW44/3	445	1985	-22.7883	167.2383	1120	620	2010	left	0.5	1	1
55918	532	2005	-20.0977	160.3718	241	120	610	right	0	0	0
55919	672	2005	-21.0847	160.7903	141	70	450	right	0	0.5	1
DW33/1	680	1985	-23.1618	167.1712	6520	6410	6660	right	1	1	1
DW33/2	680	1985	-23.1618	167.1712	5211	5070	5330	left	1	0.5	1
CP232	775	1987	-21.5635	166.4512	227	110	320	left	0.5	0	1
CP30/2	1140	1985	-23.1608	166.6808	4007	3880	4130	right	0.5	1	1
CP30/3	1140	1985	-23.1608	166.6808	500	270	1050	right	0.5	1	1
CP30/5	1140	1985	-23.1608	166.6808	1577	1450	1700	right	1	1	1
CP30	1140	1985	-23.1608	166.6808	106	40	400	left	0.5	0.5	1
CP30/4	1140	1985	-23.1608	166.6808	~50000	NA	NA	left	1	1	1
CP272	1663	1987	-21.0007	166.949	166	70	500	left	0.5	0.5	1

(Tomašových et al. 2016). The reported calendar ages refer to the year when the samples were collected from the seafloor. Two specimens (AMNH 55917 and CP266) age-dated in Tomašových et al. (2016) had unknown whole-specimen preservation and were thus excluded from analyses. We thus analyze preservation in 24 shells. Seventeen new shells are illustrated (Figs. 2–5), three specimens are represented by whorl fragments (CP30/2, CP30/3, and CP30/5), and four shells (55914, 55918, 55919, 55924) were illustrated by Mapes et al. (2010a).

Assessment of Skeletal Alteration States

We assess the alteration of shells on the basis of (1) eight alteration variables scored on external surfaces of right and left flanks and (2) asymmetry in alteration between the two flanks. Two variables detect overall loss of completeness, including (1) *completeness of the body chamber* with three states (> 50% of body chamber is preserved, < 50% of body chamber is preserved, and body chamber is completely missing), and (2) *completeness of the phragmocone wall* with three states (complete phragmocone, partly preserved phragmocone, and umbilical relict). External surface preservation is targeted by six variables scored at 10× magnification on the left and right flanks of the body chamber and phragmocone. They include (1) *sheen loss* with two states (shiny or dull); (2) *discoloration* with three states (flanks with red stripes, flanks with faded brown stripes, and discolored flanks); (3) yellowish and brownish *clay-goethitic coatings* that cover external surfaces and penetrate into pores and borings, with three states (uncoated flanks, flanks with localized or patchy coatings, and fully coated flanks); (4) *dissolution* with three states (pristine flanks without or with rare signs of surficial pitting, flanks with pitted surface (< 50%), and extensively pitted flanks with grainy surfaces); (5) *bioerosion* with three states (rare or dispersed borings, frequent shallow borings, and dense network of deep borings forming rugged flanks); and (6) *encrustation* with four states (encrusters are absent, and encruster cover with < 10%,10–50%, and > 50%). Alteration scores of all variables range between 0 (pristine) and 1 (poorly preserved) (Table 1). We investigated surface preservation of nine specimens at higher magnifications (50–5000×) with the scanning electron microscope (SEM) Hitachi S-3700N. Suess et al. (2015b) reported that living shells of *N. macromphalus* are rarely colonized by epilithic foraminifers or by boring-producing endolithic foraminifers. External bioerosion and encrustation thus can be related to processes affecting cephalopods during their life, but the extent and depth of borings observed here (penetrating to the internal surface) and encrusters (barnacles, serpulids, foraminifers, and bryozoans) attached to degraded external surfaces or crossing to internal walls suggest that they formed mainly after the death. The extent of coating and encrustation typically differs between the left flank and the right flank (Figs. 2–6). Therefore, we assign the left and right flanks of each specimen either to a more pristine or to a less pristine flank. We then report the relation between postmortem age and water depth on one hand and the degree in alteration on the other hand separately for (1) more pristine and (2) less pristine flanks. In addition to the semiquantitative alteration scores, we measure the proportional cover by coatings and encrusters on each flank in a lateral view with the ImageJ software in order to quantitatively assess between-flank differences in alteration.

Analyses of Mineralogical and Chemical Composition

The specimen CP272 was used for determination of clay minerals forming the external coatings. It was washed, crushed, ground with pestle and mortar, and subsequently treated with Na acetate buffer in order to remove carbonates. The insoluble residuum was dried and oriented preparation was produced using Si-wafer as a sample holder. X-ray diffraction analyses were performed on a Bruker D8 Advance diffractometer using Cu$K\alpha$ radiation generated at 40 kV and 40 mA and a Sol-X SD detector. The beam was collimated with a slit assembly 0.3°–6 mm–0.3°–

TABLE 1.—*Extended.*

M.p.f.-discoloration	M.p.f.-encrustation	M.p.f.-bioerosion	M.p.f.-coating	M.p.f.-dissolution	L.p.f.-phragmocone completeness	L.p.f.-sheen loss	L.p.f.-discoloration	L.p.f.-encrustation	L.p.f.-bioerosion	L.p.f.-coating	L.p.f.-dissolution
0.5	0.67	0	0	0.5	0	0	1	0.3	0	0	0
0.5	0.33	0	0	0	0	1	1	0.3	0	0	0
0	0	0	0	0	0	0	0	0	0	0	0
0.5	0.67	1	1	1	0.5	1	1	1	1	1	1
0	0.33	0	0	0	0.5	1	0	0	0	0	0.5
0.5	1	0.5	0	0.5	0	1	1	0.7	0.5	0	0.5
0.5	1	1	1	0.5	1	1	1	1	1	1	0.5
0	0.33	0	0	0.5	0.5	1	1	1	0.5	0	0.5
0	0.33	0.5	0	0	0	0	0	0.3	1	0	0
0	0.33	0	0	0.5	0.5	1	0	0	0	0	0
0	0.67	1	1	0.5	0.5	1	1	1	1	1	0.5
0	0.33	0.5	0	0.5	0.5	1	1	1	1	1	0.5
0.5	0.67	1	1	0.5	1	1	1	1	1	1	1
0	0.67	0	0	0	0	0	0	0	0	0	0
0	0	0	0	0	0.5	0	0	0	0	0	0
1	0.67	1	1	1	0.5	1	1	0.3	1	1	1
1	0.33	1	1	1	1	1	1	0.7	1	1	1
0.5	0.67	0	1	0.5	0	1	1	0.3	0.5	1	1
0.5	0.33	0	1	0	1	1	1	0.3	0	1	0
0.5	0.33	0	1	0.5	1	1	1	0.3	0	1	0.5
1	0.33	0.5	1	1	1	1	1	0.3	0.5	1	1
0.5	0.67	0.5	1	1	0.5	1	1	0.7	0.5	1	1
1	0.33	1	1	1	1	1	1	0.3	1	1	1
0.5	0.33	0	1	0	0.5	1	1	0.3	0.5	1	1

0.2 mm, primary and secondary Soller slits. Recordings were carried out both in air-dried state and after vaporization with ethyleneglycol at 60°C overnight (Fig. 7). Samples were scanned from 2–50° 2θ with step size 0.02° 2θ and 0.80 seconds counting time. The chemical composition of coatings and pore infills (five measurement spots) was analyzed in two specimens (CP232 and CP30/5) with wave-dispersion X-ray microanalysis, using a Jeol JXA-8530F electron microprobe. Operating conditions were < 1 μm spot resolution, 15 kV accelerating voltage, 20 nA probe current, and ZAF correction. The natural standards used in analyses were orthoclase for K (Kα, PETL), diopside for Ca (Kα, PETL), albite for Na (Kα, TAP), kyanite for Al (Kα, TAP), olivine for Mg (Kα, TAP), hematite for Fe (Kα, LIFH), rhodonite for Mn (Kα, LIFH), and rutile for Ti (Kα, PETL). The relative standard deviation is less than ± 5 %.

Statistical Analyses

First, we assess the relationship between specimen postmortem age and water depth on one hand and specimen scores of eight alteration variables on the other hand with full and partial Spearman rank correlations (Kim and Yi 2007). Second, we explore variation in multivariate alteration among all specimens with principal coordinate analysis (PCO). Third, we test the effects of postmortem age and water depth on multivariate alteration with constrained analysis of principal coordinates (CAP, Anderson and Willis 2003). To build the distance matrix for PCO and CAP, we use Manhattan distances among individual specimens on the basis of scores of eight alteration variables. Distances among specimens in PCO plot reflect the differences in alteration independently of their age and water depth. In contrast, CAP summarizes the among-specimen variation in the alteration that can be explained by log-transformed age and log-transformed water depth, and thus allows interpreting preservation pathways (Meldahl and Flessa 1990). To identify alteration variables most responsible for the ordering of specimens along the first two PCO and CAP axes, each alteration variable is represented by a vector generated by maximizing the correlation between alteration scores of individual specimens and their ordination scores along the first two axes (Oksanen et al. 2015). The direction of the vectors reflects the highest rate of change in the score of a given alteration variable from pristine towards altered states, and the length of the vectors is scaled by their correlation with two ordination axes (i.e., variables with long vectors strongly correlate with ordination axes).

RESULTS

Surface Alteration Patterns

Minor breakage along margins of the body chamber or perforations in the phragmocone occur in all pristine shells with red stripes (Fig. 2). Seven specimens (with age between 19 and 358 years) possess almost complete phragmocones (CP105, CP42/1, 55924, CP45/1, CP45/4, 55918, and CP232) and nine specimens (with age between 106 and 581 years) show minor to moderate breakage of the phragmocone (DW43, 55914, CP45/3, DW08, DW44/1, DW44/2, 55919, CP30, and CP272). Several shells show a major phragmocone breakage (specimens in Figs. 3, 4, 5A–5D) and three specimens show partial or almost complete removal of one of the flanks (Fig. 5E–5P). One specimen is represented by an umbilical relict (Fig. 5Q–5S). Discoloration ranges from well-preserved, shiny shells with reddish stripes to shells with faded, brownish color stripes, and finally to shells without any stripes. The color stripes are visible in thin sections as 0.1–0.2 mm-thick reddish bands in the upper parts of the external spherulitic-prismatic layer in shells (Fig. 6A–6C). In six specimens from the mesobathyal zone with external coatings, thin-sections show that coatings cover the color stripes. Therefore, although the surface of coated shells tend to be bored and dissolved, they did not fully lose their color patterns.

The coatings are represented by yellowish or brownish, 10–100 μm-thick aggregates of clays (chlorite, muscovite, and/or illite), goethite, and silt-sized detritic grains of plagioclase and quartz (Fig. 7A), coccoliths

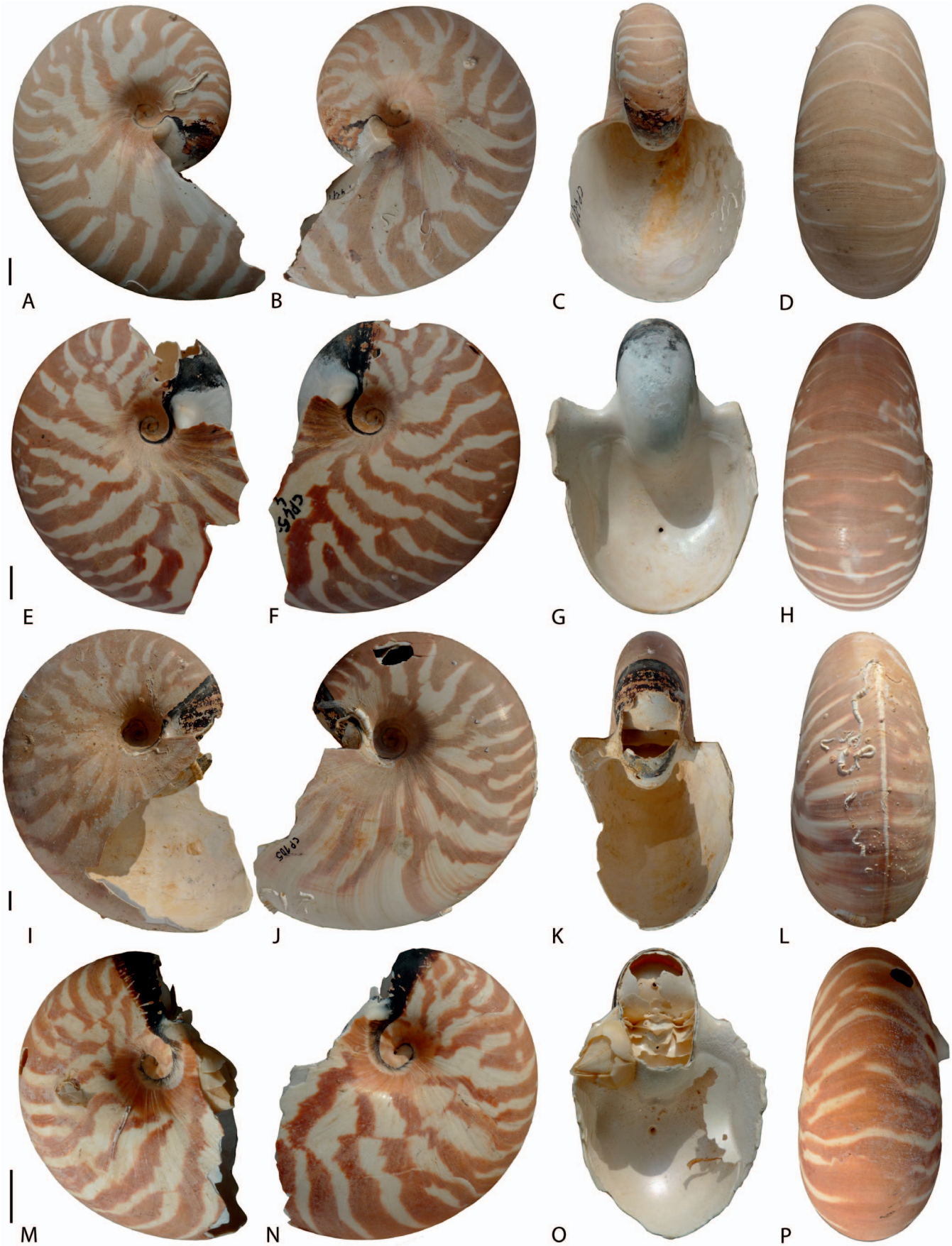

FIG. 2.—Right and left lateral, dorsal and ventral views of well-preserved specimens of *N. macromphalus*, with postmortem age ranging between 97 and 280 years. **A**–**D**) CP 42/1 (97 years), Norfolk Ridge. **E**–**H**) CP 45/4 (122 years), SW of Isle of Pines. **I**–**L**) CP 105 (245 years), E slope of New Caledonia, Loyalty Basin. **M**–**P**) DW 08 (280 years), between Ouvea and Lifou. Scale bar = 10 mm.

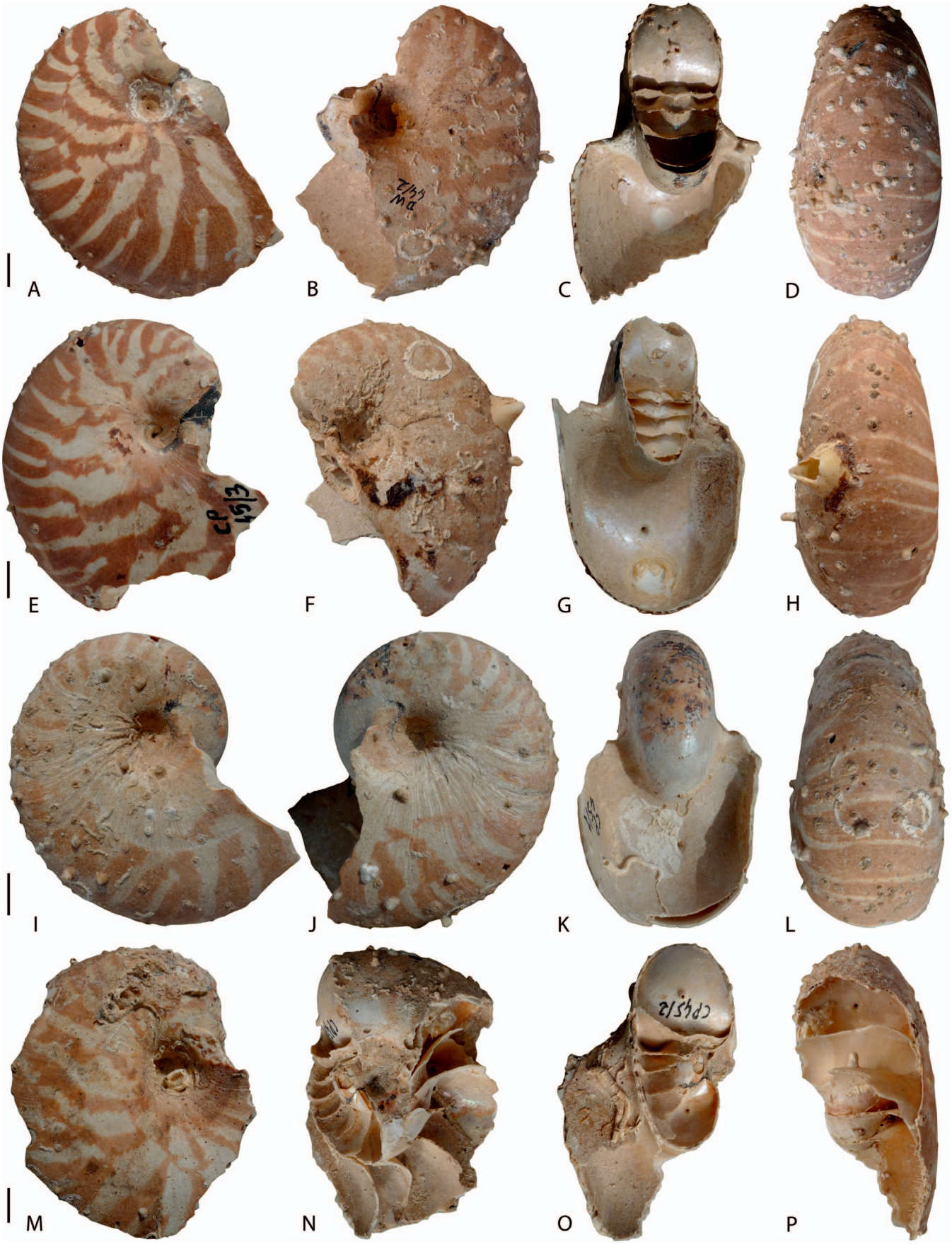

FIG. 3.—Right and left lateral, dorsal and ventral views of moderately altered specimens of *N. macromphalus*, with postmortem age ranging between 173 and 416 years. **A**–**D**) DW 44/2 (173 years), SW of Isle of Pines. **E**–**H**) CP 45/3 (416 years), SW of Isle of Pines. **I**–**L**) CP 45/1 (358 years), SW of Isle of Pines. **M**–**P**) CP 45/2 (169 years), SW of Isle of Pines. Scale bar = 10 mm.

FIG. 4.—Right and left lateral, dorsal and ventral views of *N. macromphalus* partly or fully coated by yellowish and brownish clay-goethitic coatings, with postmortem age ranging between 106 and 324 years. **A**–**D**) CP 232 (227 years), E slope of New Caledonia, Loyalty Basin. **E**–**H**) CP 30 (106 years), New Caledonia Basin, SW New Caledonia. **I**–**L**) DW 44/1 (324 years), SW of Isle of Pines. **M**–**P**) CP 272 (166 years), Loyalty Basin, W of Lifou. Scale bar = 10 mm. We note that CP272 was affected by a secondary post-collection damage.

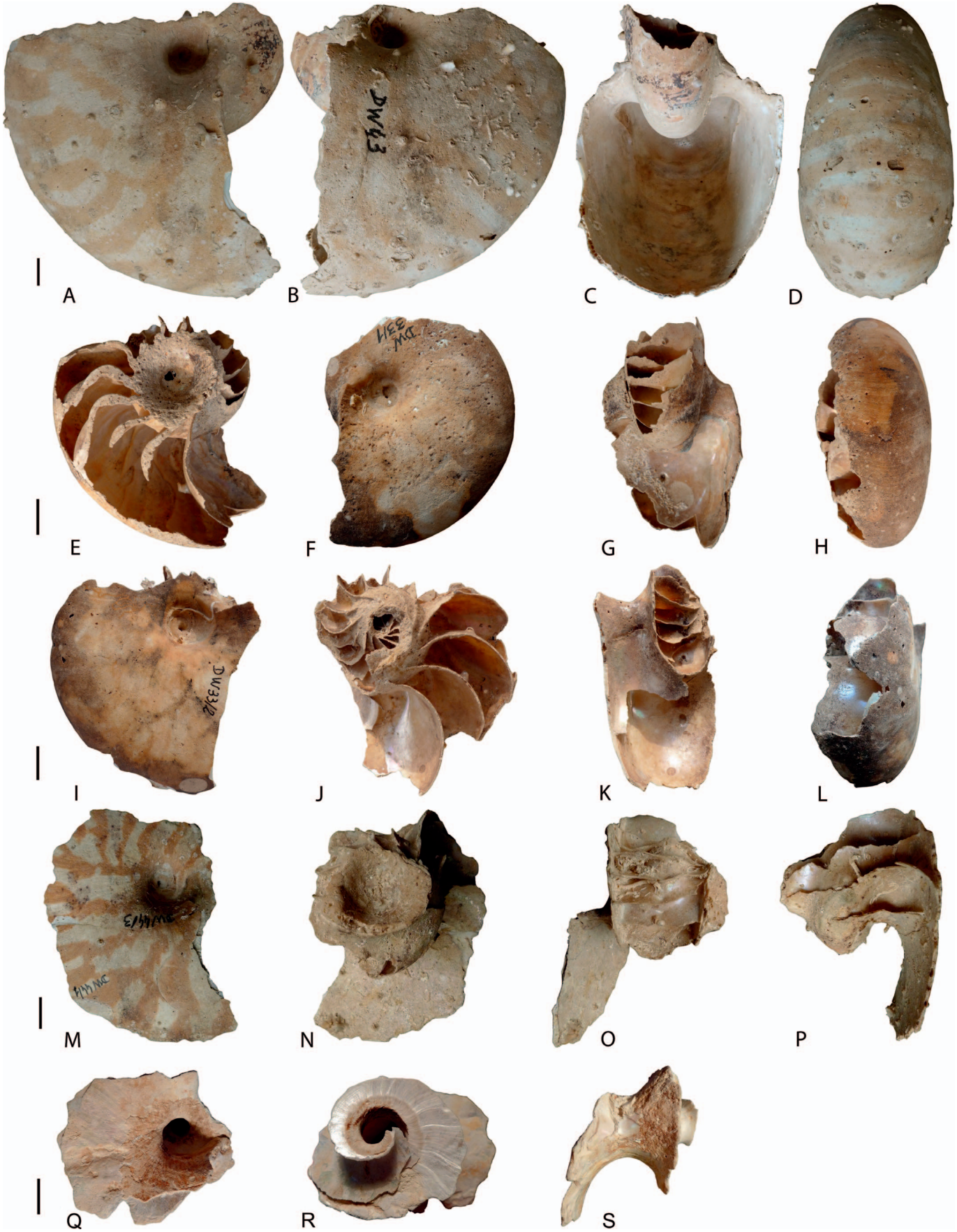

FIG. 5.—Right and left lateral, dorsal and ventral views of poorly preserved and old specimens of *N. macromphalus*, with postmortem age ranging between 581 and 6520 years. The specimen CP 30/4 is at least 50,000 years old. **A**–**D**) DW 43 (581 years), SW of Isle of Pines. **E**–**H**) DW 33/1 (6520 years), SW of Isle of Pines. **I**–**L**) DW 33/2 (5211 years), SW of Isle of Pines. **M**–**P**) DW 44/3 (1120 years), SW of Isle of Pines. **Q**–**S**) Right lateral, and two internal views of CP 30/4 (~ 50,000 years), New Caledonia Basin, SW New Caledonia. Scale bar = 10 mm.

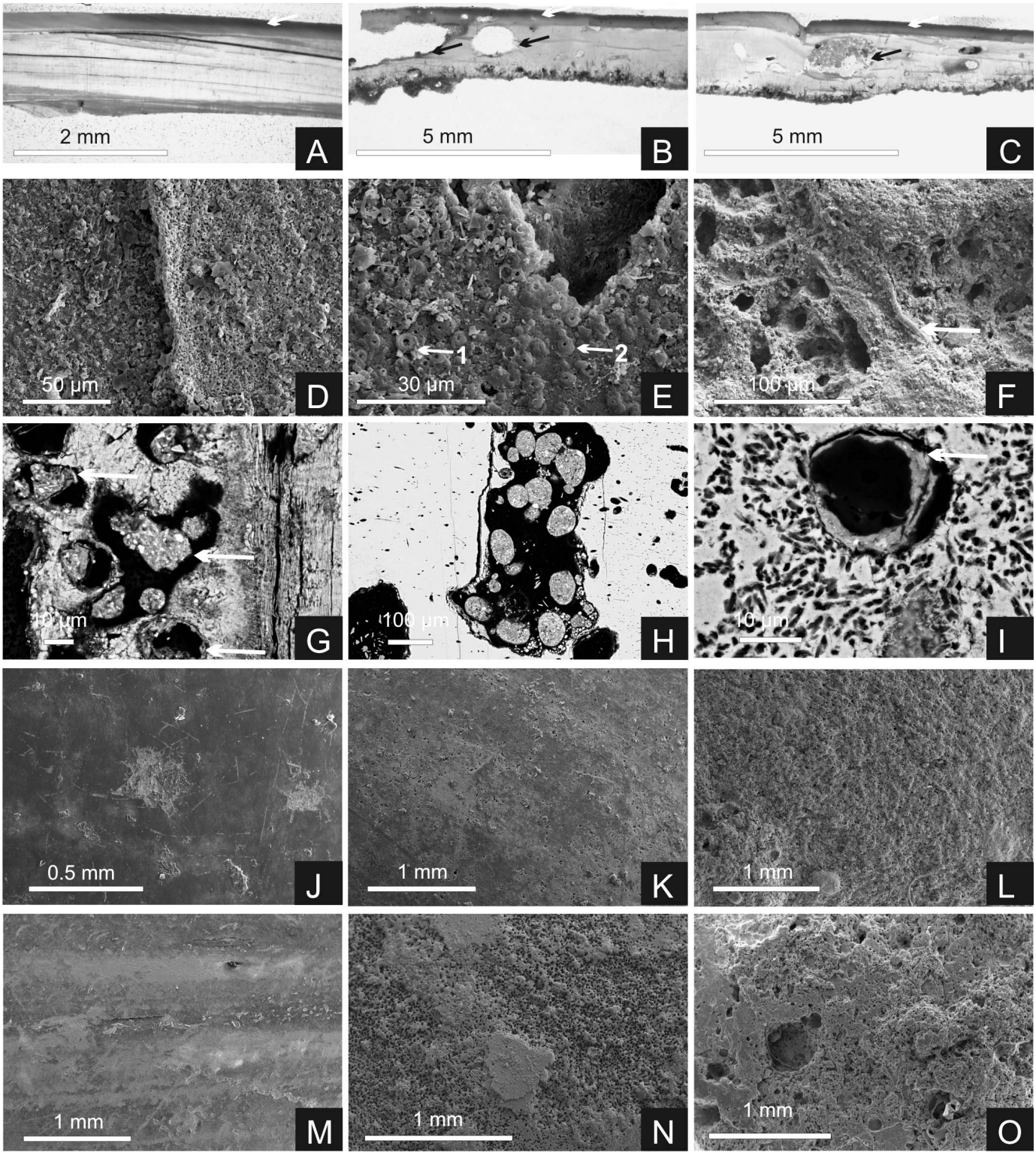

FIG. 6.—Progression of bioerosion and dissolution and the appearance of coatings in cross-sections and in plane views. **A**–**C**) Cross-sections in translucent light showing color stripes in the uppermost part of the prismatic layer (white arrows) and sponge-induced channels (black arrows) in the nacreous layer (A-CP272, B-C-DW44/1, both specimens show more pristine flanks). **D**–**F**) SEM plan-views of clay coatings rich in coccoliths (white arrows: 1, complete plate; 2, dissolved relict) that cover external surfaces (D-E-CP272, left, less pristine flank) and rim microborings close to the external surface (F-CP232, left, less pristine flank, white arrow: microbial filament). **G**–**I**) Backscattered electron (BSE) images showing clay-goethitic infills and pelletal aggregates (white arrows) in sponge borings in CP 232 (G) and DW44/1 (H), and internal coatings of borings in CP30/5 (I). **J**) Pristine external surface of the left (more pristine) flank with rare microborings and incipient dissolution (dissolution state = 0, CP45/4). **K**) A relatively smooth but pitted external surface of the left (more pristine) flank associated with surficial borings (dissolution state = 0.5, CP105). **L**) Extensively pitted and grainy external surface of the right (more pristine) flank (dissolution state = 1, DW44/3). **M**) Smooth external surface of the right (more pristine) flank with surficial grazing marks and no microborings (bioerosion state = 0, CP42/1). **N**) Dense network of surficial borings on external surface of the left (less pristine) flank (bioerosion state = 0.5, CP232). **O**) Densely bored external surface forming microterraces on the left (more pristine) flank (bioerosion state = 1, DW33/1).

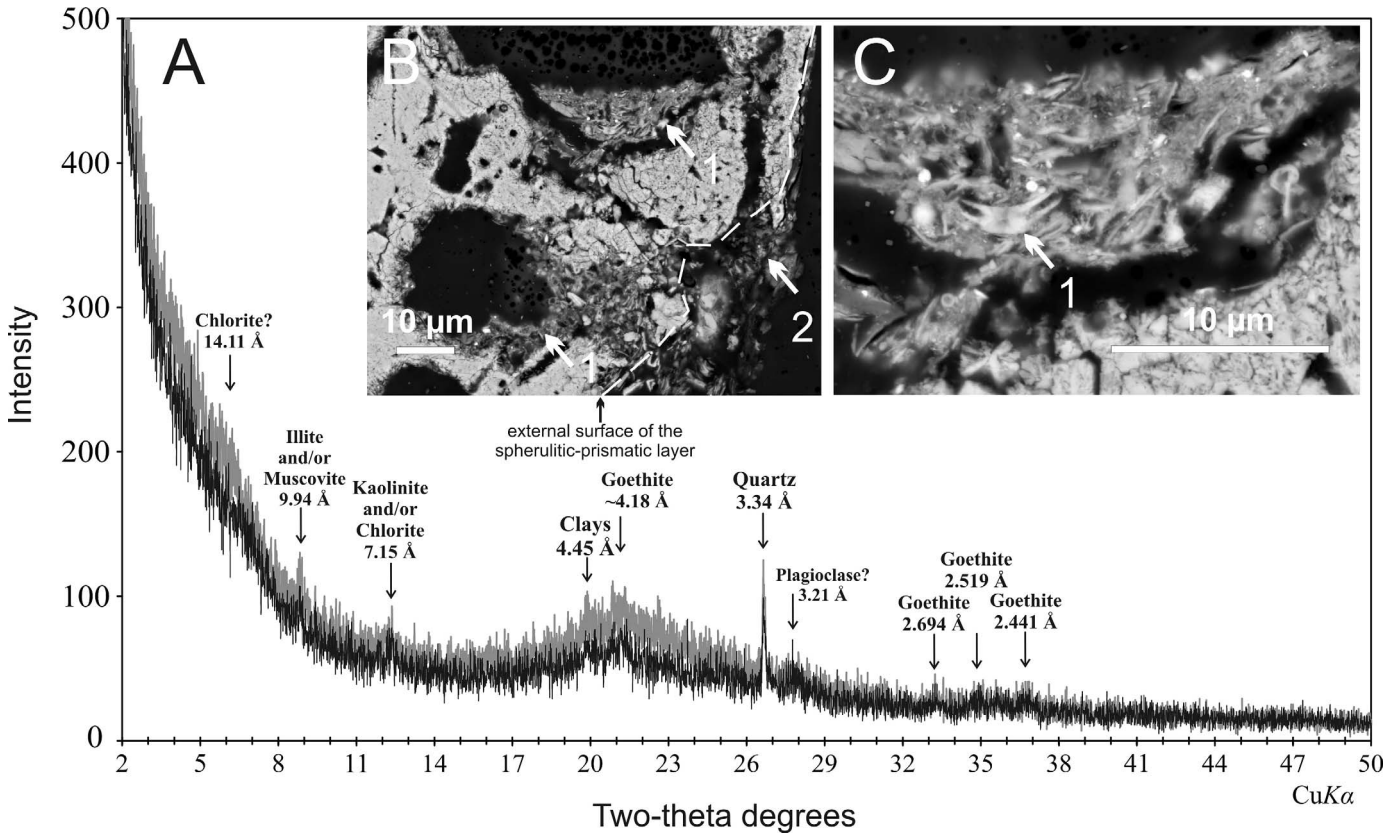

FIG. 7.—**A**) X-ray diffraction analysis of external coating shows that it mainly consists of clay minerals and goethite. Intensity records are based on air-dried state (black line) and after vaporization with ethyleneglycol at 60°C overnight (gray line). **B**) Backscattered electron (BSE) images showing clay-goethitic boring infills (arrow 1) and external coatings (arrow 2). **C**) Close-up view of B shows cross-sections of coccolith plates (arrow).

(Fig. 6D, 6E), and microbial filaments (Fig. 6F). These clay-goethitic coatings are either preserved as thin crusts on the outer walls (Fig. 6D, 6E, 7B, 7C), as fillings or aggregated pellets in sponge chambers and borings (Fig. 6G, 6H), or as gravity-defying coatings, completely or incompletely rimming boring chambers (Fig. 6I, 7B). Although some coccoliths are represented by complete plates (arrow 1 in Figs. 6E, 7C), the majority of plates is represented by dissolved relicts (arrow 2 in Fig. 6E). The chemical composition of the structureless clay matrix among detritic grains demonstrates high contributions of Fe, Si and Al and low contributions of Mn (averages based on five measurements, CP232: $SiO_2 = 29\%$, $Al_2O_3 = 17\%$, $FeO_{total} = 27.8\%$, $K_2O = 1.6\%$, $Na_2O = 0.7$, $CaO = 1.6\%$, $MgO = 3.1\%$, $MnO = 0.3\%$, $TiO_2 = 0.6\%$; CP30/5: $SiO_2 = 42.6\%$, $Al_2O_3 = 22\%$, $FeO_{total} = 8.7\%$, $K_2O = 2.34\%$, $Na_2O = 0.32$, $CaO = 2.9\%$, $MgO = 3.2\%$, $MnO = 0.12\%$, $TiO_2 = 0.65\%$).

Fine-scale dissolution is coupled with microbioerosion when observed at high magnifications (Fig. 6J–6L). Some specimens from the mesobathyal zone are less extensively bored than the epibathyal shells but they are chalky and show extensive pitting. Bioerosion is represented by surface grazing marks that remove the surficial sheen (Fig. 6J), by mm-scale traces and scars left after encrusting foraminifers, and by large mm-scale chambers and tunnels (Figs. 6B, 6C, 8). The mm-scale chambers are characteristic of the central excavation structures produced by sponges of the genus *Aka* (Calcinai et al. 2007). These chambers are 0.5–5 mm-long, are preferentially located in the middle nacreous layer, and protrude with canals or tunnels into the internal and external prismatic layers (Fig. 8A–8D). The chambers are frequent on whorl cross-sections in all nine epibathyal specimens affected by shallow or deep bioerosion (the other eight epibathyal specimens show no or minor bioerosion). The mesobathyal specimens do not show such large chambers, but also possess concentric etching marks typical of the sponge *Aka* (Fig. 8A–8E) (Calcinai et al. 2004). Some chambers still contain bundles of spicules (Fig. 8F). These observations indicate that sponge bioerosion represents the volumetrically most dominant type of bioerosion in dead *Nautilus* shells from epi- and mesobathyal zones, and strongly contribute to disintegration of *Nautilus* in the epibathyal zone.

Encrusters are represented by barnacles (Fig. 3H), bryozoans, serpulids (Figs. 2L, 4L), solitary corals (Fig. 4H), sponges, agglutinated foraminifers (*Placopsilina* cf. *bradyi*, Fig. 8G), and calcareous foraminifers mainly represented by *Lobatula lobatula* (Fig. 8H, 8I) and arborescent species (Fig. 3D, 4L). Foraminifers vary in preservation, ranging from complete tests up to severely worn and eroded relicts and scars (Fig. 8H, 8I).

Relationship Between Postmortem Age and Univariate Preservation

The alteration scores of most variables tend to increase with postmortem age in both epibathyal and mesobathyal shells, on both more pristine (white boxplots in Fig. 9) and less pristine flanks (gray boxplots in Fig. 9). Heavily degraded shells younger than ~ 200 years are absent. Mesobathyal shells are not shiny, do not possess fully preserved red stripes and are at least partly coated, and thus do not capture the full spectrum of alteration states. The increase in alteration with postmortem age is thus weaker in mesobathyal shells. With the exception of encrustation, six variables show moderately high positive and significant correlations with age in full and partial Spearman rank correlations, and bioerosion shows positive correlations of borderline significance (Table 2). The extent of clay-goethitic coating significantly increases with water depth in full and partial

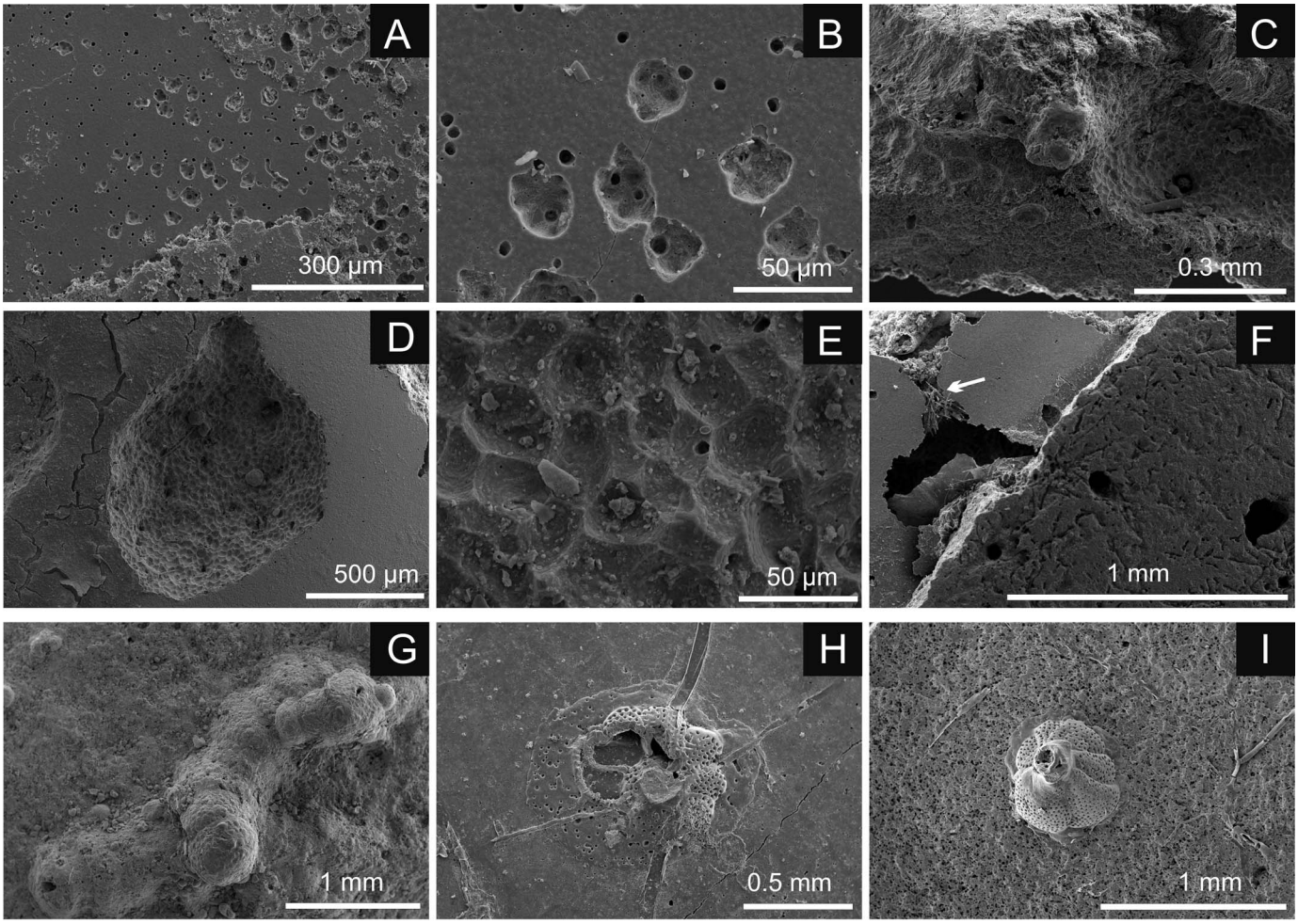

FIG. 8.—Sponge bioerosion in the nacreous layer and encrusters. **A**, **B**) Boring of sponges (*Aka*) in the nacreous layer, with concentric etching marks (CP272). **C**) Central chambers of *Aka* located in the nacreous layer (DW44/3). **D**, **E**) Central chamber in the nacreous layer in plan views with concentric etching marks (DW43). **F**) The bundle with sponge spicules (arrow) located on the margin of the central chamber (DW44/3). **G**) *Placopsilina* cf. *bradyi* Cushman and McCulloch 1939 on the external surface of the right (more pristine) flank (DW44/3). **H**) Poorly preserved *Lobatula lobatula* (Walker and Jacobs 1798), with feeding tubes, on external surface of right (less pristine) flank (CP105). **I**) *Lobatula lobatula* attached to extensively bored internal surface (DW43).

rank correlations (Table 2). On less pristine flanks, dissolution and fragmentation of body chamber and phragmocone correlate positively with water depth (Table 2). Finally, the rate of increase in alteration with postmortem age varies among variables (Fig. 9): median age of shells fully losing sheen and attaining extensive bioerosion and encrustation (several centuries in the epibathyal and mesobathyal zones) is younger than median age of shells with full discoloration ($>$ 1,000 years) or full clay-goethitic coatings ($>$ 1,000 years in the epibathyal zone but few centuries in the mesobathyal zone). The median age of heavy surface degradation due to deep bioerosion is few centuries in the epibathyal zone but approximately millennia in the mesobathyal zone.

Relationship Between Postmortem Age and Multivariate Preservation

The first PCO axis explains 67–70% of variation in alteration of more pristine and less pristine flanks, respectively (Table 3), and orders shells according to their postmortem age (Fig. 10A, 10B). The Pearson correlation between the first PCO axis and postmortem age of shells is relatively high ($r = 0.71$–0.68, $p < 0.001$), also showing that variation in alteration principally co-varies with variation in postmortem age. Vectors of alteration variables fitted to PCO show that they all increase along the first PCO axis (gray arrows in Fig. 10B). Variation in alteration is explained by log-transformed age (41–39% of variation in alteration of more pristine and less pristine flanks explained) and by log-transformed water depth (19–20% of variation explained) (Fig. 10C, 10D, Table 3). The two predictors—age and water depth—explain together 46–45% of variation in alteration. With the exception of encrustation, all alteration variables progress towards more altered states along the first CAP axis, and similarly as in PCO, this axis reflects an increase in postmortem age (dashed contours in Fig. 10C, 10D). CAP axis 2 correlates positively with water depth. Positive coordinates correspond to partly discolored and coated shells represented by the mesobathyal shells (CP232, CP272, and CP30) whereas negative coordinates correspond to encrusted and bored epibathyal shells. CAP thus reveals the presence of two postmortem pathways, with faster encrustation and strong bioerosion in the epibathyal zone (gray arrow on the bottom) and with faster growth of clay-goethitic coating and faster dissolution in the mesobathyal zone (black arrow on the top) (Fig. 10D). Both pathways converge towards similar alteration states characterized by bored and dissolved relicts.

Asymmetric Preservation and Half-Shells

Both flanks tend to be well preserved in very young shells, with original color patterns preserved (Fig. 2). However, flanks of several intermediate-

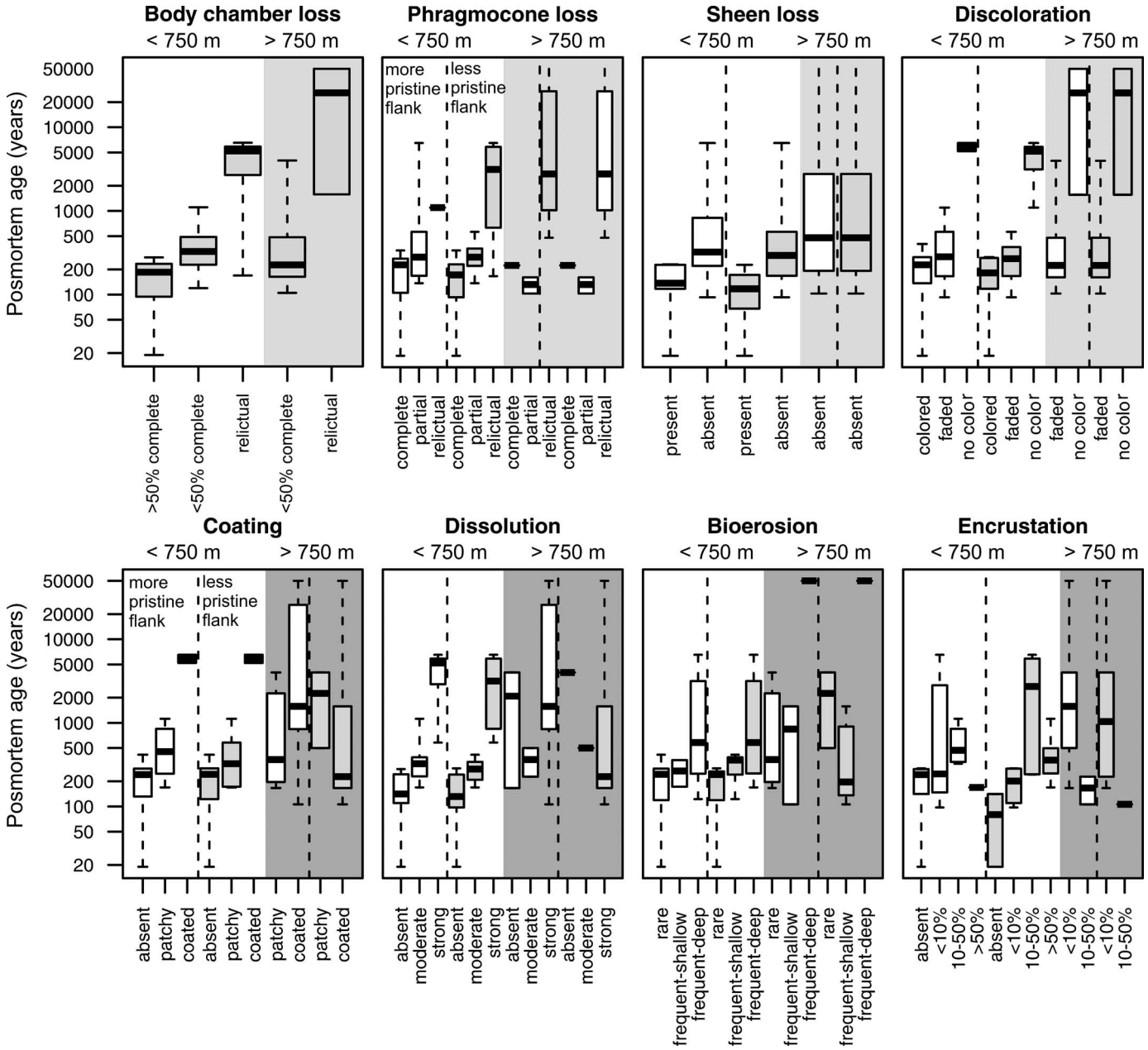

FIG. 9.—Boxplots show that the degree of incompleteness of body chamber and phragmocone, and the degree of sheen loss, discoloration, coating, dissolution, and bioerosion increase with increasing postmortem age, separately for shells sampled in the epibathyal zone (< 750 m, plot portions with white background) and mesobathyal zone (> 750 m, plot portions with gray background), and separately for more pristine (boxplots with white color) and less pristine flanks (boxplots with gray color). Shells from the mesobathyal environments do not capture all alteration states.

age specimens highly differ in the degree of encrustation in epibathyal shells and in the degree of clay-goethitic coating in mesobathyal shells (Fig. 11). Such shells that differ in alteration scores between two flanks, especially in the degree of encrustation and coating, are ~ 200–500 years old. One of the flanks is partly or completely lost in the oldest shells (Fig. 12).

DISCUSSION

Preservation Pathways

Univariate and multivariate analyses demonstrate that variation in postmortem age explains a moderately high amount of variation in alteration patterns, and that this variation can be used as a taphonomic clock in chambered cephalopods. PCO 1 and CAP 1 effectively reflect temporal progression of alteration pathways, allowing us to reconstruct the sequence of alteration events in the epibathyal and mesobathyal zone (Fig. 10, Tables 2, 3). First, preservation pathways in the epibathyal zone start with the loss of sheen, initial fragmentation of body chamber and phragmocone (occurring over multiple decades), progress with partial discoloration, encrustation, and extensive sponge-induced bioerosion (occurring over centuries), and terminate with full discoloration, extensive surface alteration due to bioerosion and dissolution, fragmentation of flanks, and formation of clay-goethitic coatings (> 1,000 years). In the mesobathyal zone, shells accrue clay-goethitic coatings, discoloration and

TABLE 2.—*Spearman rank correlations for the relationship between alteration scores of eight variables on one hand and postmortem age and water depth on the other hand, separately for more pristine and less pristine flanks. Full correlations are in the top and partial correlations are in the bottom.*

	More pristine flank-age-**full** r	p value	Less pristine flank-age-**full** r	p value	More pristine flank-depth-**full** r	p value	Less pristine flank-depth-**full** r	p value
Body chamber loss	0.59	0.002	NA	NA	0.5	0.014	NA	NA
Phragmocone loss	0.59	0.002	0.68	0.0003	0.57	0.0038	0.55	0.0058
Sheen loss	0.47	0.021	0.41	0.047	0.33	0.12	0.24	0.26
Discoloration	0.55	0.005	0.67	0.0004	0.43	0.036	0.4	0.05
Staining	0.54	0.006	0.41	0.046	0.68	0.0002	0.75	<0.0001
Dissolution	0.58	0.003	0.47	0.022	0.3	0.15	0.47	0.021
Bioerosion	0.38	0.07	0.39	0.060	0.05	0.82	0.16	0.45
Encrustation	0.13	0.54	0.27	0.21	0.06	0.78	-0.23	0.28
	More pristine flank-age-**partial** r	p value	Less pristine flank-age-**partial** r	p value	More pristine flank-depth-**partial** r	p value	Less pristine flank-depth-**partial** r	p value
Body chamber loss	0.52	0.005	NA	NA	0.39	0.05	NA	NA
Phragmocone loss	0.52	0.005	0.63	0.0002	0.49	0.01	0.46	0.02
Sheen loss	0.4	0.045	0.36	0.08	0.21	0.33	0.12	0.58
Discoloration	0.48	0.011	0.62	0.0003	0.31	0.13	0.26	0.22
Staining	0.45	0.019	0.26	0.220	0.63	0.0002	0.71	<0.0001
Dissolution	0.53	0.004	0.37	0.070	0.14	0.52	0.37	0.06
Bioerosion	0.39	0.050	0.36	0.073	-0.09	0.67	0.04	0.87
Encrustation	0.12	0.58	0.37	0.060	0.02	0.93	-0.35	0.08

dissolution earlier, and encrustation and bioerosion are less extensive than in the epibathyal zone (Fig. 9). The formation of coatings probably reflects trapping of detrital sediment coupled with the growth and metabolism of microorganisms that bound sediment particles into cohesive mats (as suggested by gravity-defying rims) or pellets. Second, preservation pathways are associated with differential accrual of alteration on upward-oriented flanks exposed to colonization by encrusters and borers and downward-oriented flanks protected from alteration (Figs. 11, 12). Some pathways can generate similar outcomes. For example, surficial alteration caused by grazers, bioeroders, and dissolution generates sheen loss (Fig. 6L, 6O), and the loss of the uppermost shell layers due to bioerosion or dissolution contributes to discoloration. The sole alteration variable unrelated to age is represented by encrustation. Although the degree of encrustation initially increases with postmortem age, the oldest shells show low percent cover by encrusters (Figs. 9, 11), possibly due to extensive surface degradation and erosion of previously attached encrusters (Fig. 8H) (Richardson-White and Walker 2011).

Effects of Depth

Environmental variation in alteration and disintegration rates can have strong effects on frequency of alteration states (Parsons-Hubbard 2005; Best 2008; Powell et al. 2011, 2012; Ritter et al. 2013). Here, we have found that differences in water depth explain a significant amount of variation in postmortem preservation (Tables 2, 3), primarily separating epibathyal and mesobathyal shells along the axis 2 in PCO and CAP analyses (Fig. 10). Multiple environmental factors affecting preservation can vary with depth, and it can be difficult to disentangle their effects. *Nautilus* shells lose color and are corroded and encrusted by algae, cyanobacteria and epibionts in nearshore environments (Mapes et al. 2010b), but bathyal pathways observed here are more dominated by damaging activities of heterotrophic organisms and by sea-floor early diagenetic processes. Here, we suggest that the difference in alteration between epibathyal and mesobathyal zones off New Caledonia can reflect bathymetric decrease in primary productivity (Lescinsky et al. 2002; Wisshak et al. 2015) and bathymetric increase in bottom-water saturation (Gerhardt and Henrich 2001). On one hand, secondary production of suspension-feeders in the epibathyal zone off New Caledonia is markedly larger than in the mesobathyal zone (Roux et al. 1991), and the higher levels of sponge bioerosion and encrustation in the epibathyal zone can thus reflect a higher food supply at such depths. The major pathways leading to disintegration of *Nautilus* shells in the epibathyal zone are caused by the excavating sponge *Aka* (Figs. 6B, 6C, 8A–8F), ultimately leading to the collapse of flanks and heavy fragmentation so that most epibathyal shells disintegrate to unidentifiable relicts over few centuries (Tomašových et al. 2016). The higher colonization rates of dead shells by grazers, encrusters and borers in the epibathyal zone could also delay or disable the formation of clay-goethitic coatings. On the other hand, mesobathyal specimens occur close or below the aragonite compensation

TABLE 3.—*Multivariate analyses showing the amount of multivariate variation in alteration explained by the principal component analysis (PCO), Pearson correlation effects between PCO axes, water depth and postmortem age, and the effects of log-transformed age and log-transformed depth on multivariate variation in alteration as detected by constrained analysis of principal coordinates (CAP), separately for more and less pristine flanks.*

	More pristine flank	*p* value	Less pristine flank	*p* value
Principal coordinate analysis				
% explained by PCO axis 1	0.67	NA	0.7	NA
% explained by PCO axis 2	0.11	NA	0.12	NA
Pearson correlation between PCO axis 1 and shell age	0.71	<0.001	0.68	<0.001
Pearson correlation between PCO axis 2 and water depth	0.55	0.005	0.67	<0.001
Constrained analysis of principal coordinates				
Multivariate alteration~age+depth	0.46	<0.001	0.45	<0.001
Multivariate alteration~age	0.41	<0.001	0.39	<0.001
Multivariate alteration~depth	0.19	0.022	0.2	0.02

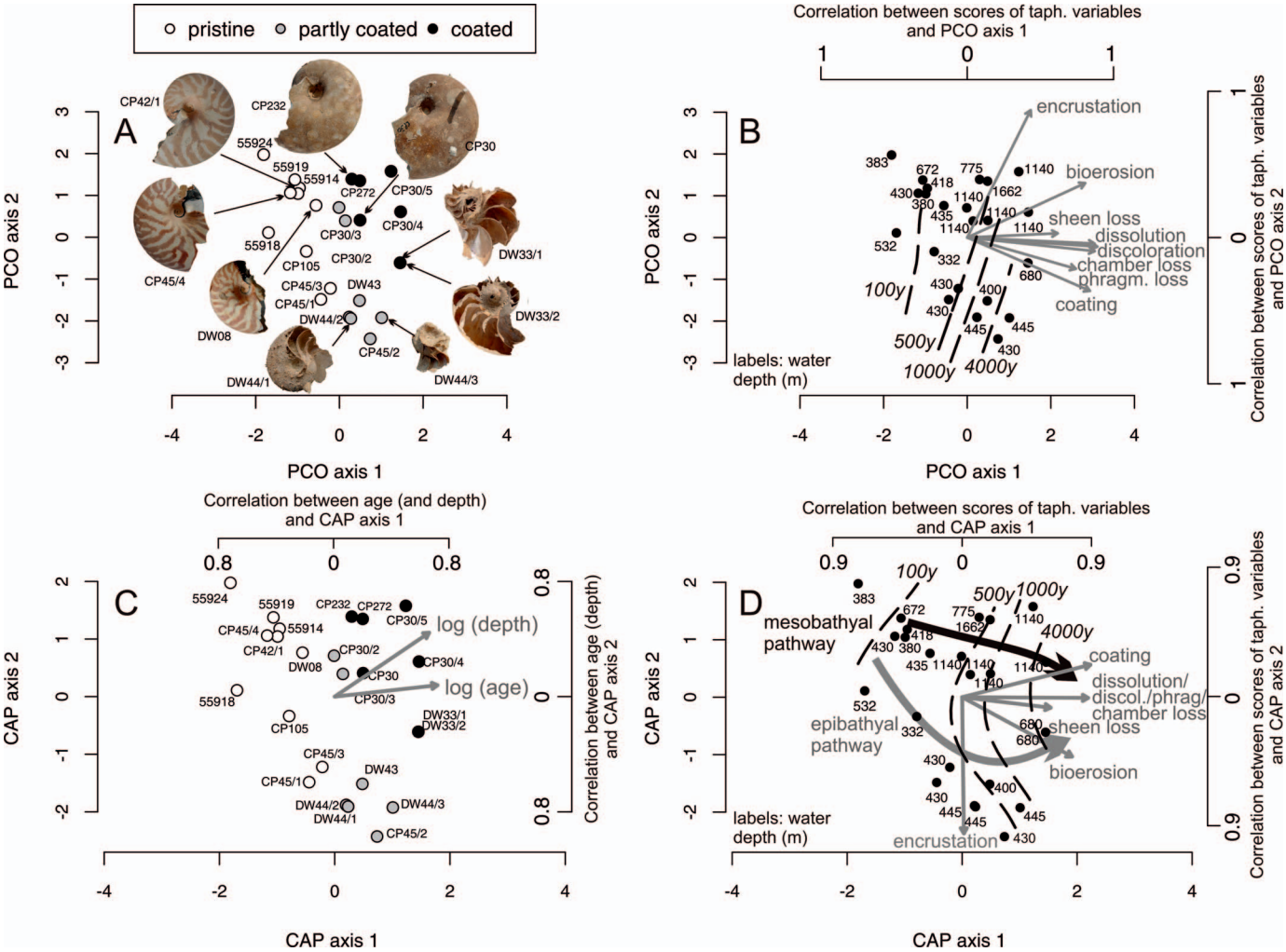

FIG. 10.—Principal coordinate analysis (PCO, A-B) and constrained analysis of principal coordinates (CAP, C-D) visualize preservation pathways of shells with increasing postmortem age in two depth zones. Both analyses are based on alteration of less pristine flanks. They show that the overall alteration and specimen postmortem age tend to increase towards the positive values along the first PCO and CAP axes. CAP analyses in C and D show that water depth increases towards the upper right corner, and the combined effect of age and depth can be visualized by two (epibathyal and mesobathyal) pathways. In both rows, the left panel shows specimen identification numbers and specimen symbols are coded according to their degree of coating. The right panel shows specimens identified by water depth in meters, black-line dashed contours represent approximate postmortem age of these specimens fitted by generalized additive models, and vectors of eight taphonomic variables (their correlation with axes 1 and 2 is shown on the top side and the right plot sides, respectively). The direction of these vectors reflects the steepest gradient from pristine towards altered states and their length is scaled by their correlation with two ordination axes. We note that some specimens share the same coordinates in PCO and CAP plots.

depth that is located at 1,100–1,200 m in this region (Feely et al. 2002). The higher dissolution levels and earlier onset of surficial dissolution and discoloration in the mesobathyal zone (Fig. 9) can reflect the effect of lower bottom-water saturation, and thus a higher contribution of dissolution to disintegration in the mesobathyal zone. Higher dissolution could generate bathymetric increase in disintegration rates but it is likely that the decline in bioerosion counteracts such trend because three specimens older than 1,000 years still occur at depth 1,140 m.

Effects of Sea-Floor Stability, Asymmetric Preservation, and Preservation of Half-Shells

The preservation of cephalopod half-shells, with the preservation of single flanks with septal relicts, is characteristic of many fossil assemblages from the Mesozoic (Seilacher et al. 1976; Tanabe et al. 1984; Olóriz et al. 2002, 2004). Specific pathways that generate such preservation can vary among environments. For example, Maeda (1987) suggested that a drift-through current allowed partial infill of chambers by the deposition of sediment reaching below the septal necks. In such case, the naked septa were prone to dissolution and led to the collapse of the upper shell flank. In our study, disintegration and collapse of the upper flank proceeds simultaneously with septal disintegration due to sponge-induced bioerosion. The sediment infill is thus not limited by the position of septal necks in the New Caledonia assemblages because phragmocones are frequently broken or penetrated by borings. However, all such occurrences likely share three key characteristics: (1) shells must be oriented in a horizontal position on the sea-floor; (2) the opposing flanks must be exposed to different taphonomic regimes (with one flank exposed to the TAZ and another flank exposed to the less reactive SZ) (Tomašových et al. 2014); and (3) the same polarity of the right and left flanks should persist for a relatively long temporal duration. Although dead shells of *Nautilus* exposed on the sea-floor can be highly susceptible to reorientation or transport under moderate intensity of bottom currents (Wani and Ikeda 2006) the between-flank difference in preservation in intermediate-age

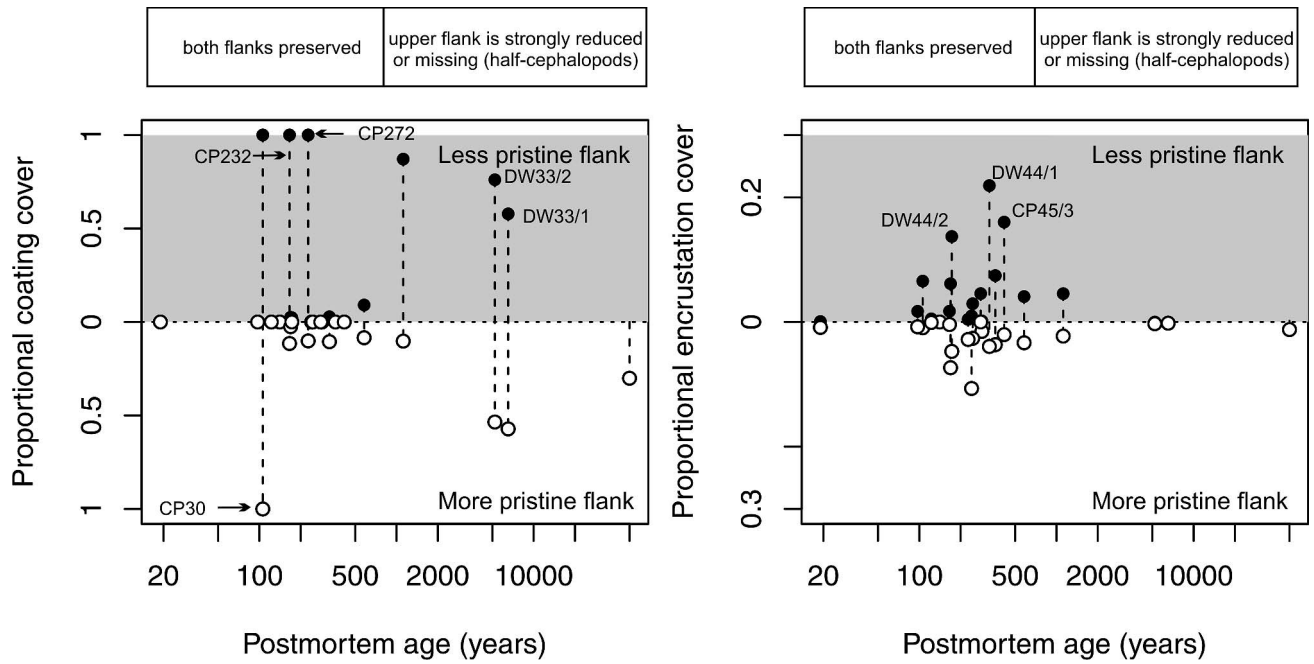

FIG. 11.—Asymmetry in shell preservation comparing proportional cover of brownish coatings (A) and encrusters (B) between the less pristine flanks (top gray sector) and the more pristine flanks (bottom white sector). The flanks belonging to the same specimens are connected by vertical dashed lines. The alteration score of the less pristine flank increases along the y-axis towards the top, whereas the alteration score of the more pristine flank increases in a reverse direction towards the bottom. The plots show that shells with highly asymmetric preservation (and both flanks preserved) are centuries old and relicts with one flank removed are millennia old. Specimens CP232, CP272, and DW44/3 are fully coated just on one side.

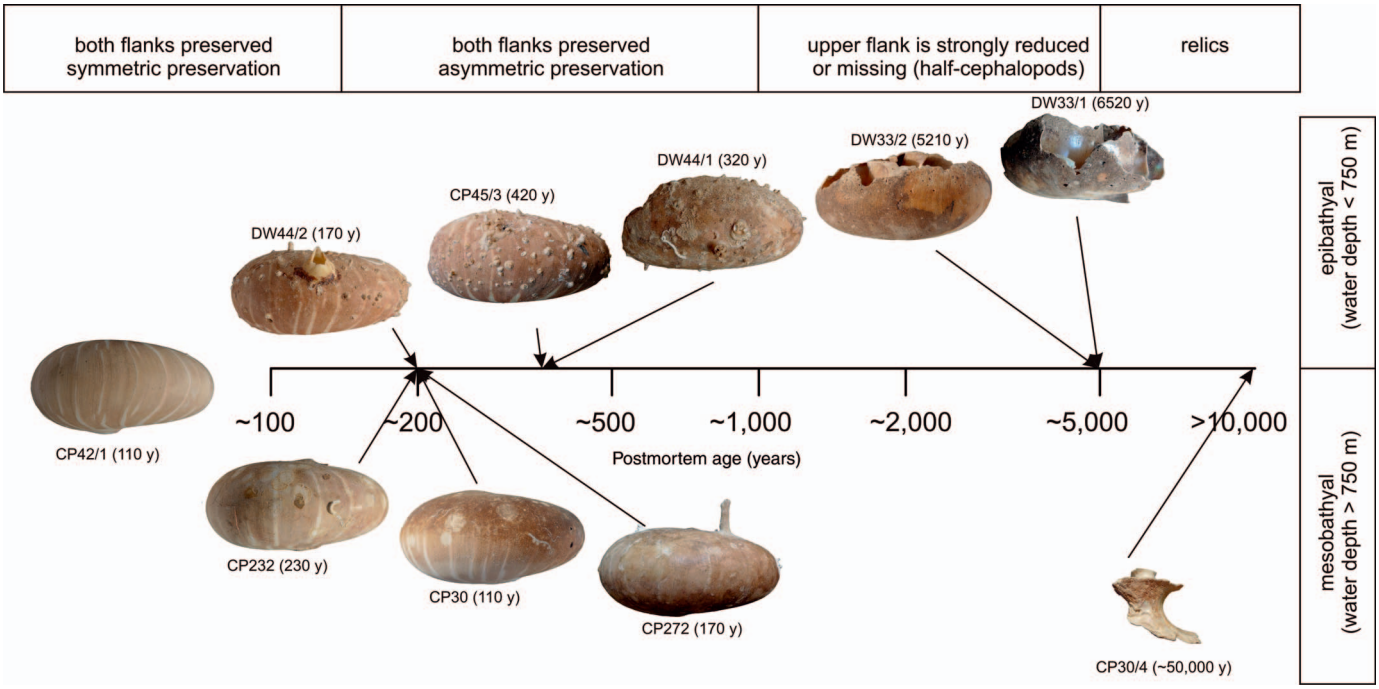

FIG. 12.—Age- and depth-dependence in external surface alteration and in asymmetry of alteration. The epibathyal pathway is dominated by encrustation and bioerosion, with a discoloration and full coating occurring at millennial scales. The mesobathyal pathway leads to a full coating after few centuries and to smaller encrustation and bioerosion. Asymmetry is visible in differential encrustation and bioerosion of two flanks in the epibathyal zone and in the differential coating of two flanks in the mesobathyal zone. The oldest shells in the epibathyal zone are represented by relict half-shells.

Nautilus shells and the lack of one of the flanks in the oldest *Nautilus* shells (Figs. 11, 12) imply negligible physical and biotic sediment mixing at decadal or centennial scales and the lack of strong bottom currents. Deep-shelf or bathyal environments can generally provide more appropriate conditions for the use of the taphonomic clock than those in shallow environments because bioturbation rates and depth of bioturbation tend to decline with decreasing flux of particulate organic carbon (Trauth et al. 1997) and with increasing depth (Middelburg et al. 1997). Under slow bioturbation, burial of shells to the SZ and their subsequent exhumation back to the TAZ, and thus decoupling between postmortem age and alteration, is less likely.

Detecting Scales of Time Averaging on the Basis of Cephalopod Preservation

In the fossil record, accumulations with cephalopods are preserved as census and within-habitat time-averaged assemblages (Wani 2001; Tomašových and Schlogl 2008; Cichowolski et al. 2012), multiple-habitat time-averaged assemblages (Fernandez-Lopez 2011; Nieto et al. 2012), and biostratigraphically condensed assemblages preserved on sediment-starved, pelagic swells (Martire 1992; Santantonio 1993; Reolid et al. 2010). Nautiloid assemblages observed here primarily reflect within-habitat time-averaged assemblages because most shells are not older than few centuries and depositional and oceanographic conditions were relatively stable over the last centuries and millennia in the southwestern Pacific (Mamo et al. 2013; Gagan et al. 2004). The six oldest shells (thousand years old) mark the transition to assemblages averaged across multiple habitats, but their proportional contribution to the total assemblage is relatively small (25%).

Although bathymetric effects clearly confound taphonomic clock estimates, variation in the degree of sheen loss, discoloration, sponge bioerosion, and clay-goethitic coatings can segregate fossil cephalopod shells on the basis of preservation into distinct age groups in sediments occurring at epibathyal depths (above the effects of aragonite compensation depth). First, sheen and color preservation, frequently preserved in fossil chambered cephalopods (Mapes and Larson 2015), can be used as an evidence of within-habitat time averaging (multiple decades to few centuries) because their loss occurs at relatively high rates, similarly as observed in other studies (Wilson 1988; Powell and Davies 1990; Wehmiller et al. 1995). Second, extensive and deep bioerosion in bathyal environments, especially when produced by excavating sponges that can be also detected in thin-sections, imply longer, centennial exposure on the sea-floor and environmental condensation. We note that the rate of sponge bioerosion tends to be much higher on shelves than in bathyal zones (Wisshak et al. 2011), and sponge-induced damage thus can be a less sensitive tool for discrimination of yearly/decadal-scale from centennial-scale time averaging in shallow-water fossil assemblages. Third, fully developed clay-goethitic coatings indicate millennial exposure on the epibathyal sea-floor and environmental or even biostratigraphic condensation, most likely because the input of goethite is very limited over shorter time scales. The overall chemical composition with high concentrations of Si, Al, and Fe, abundance of rims and pellets in semi-enclosed borings, and coccolith dissolution suggest that these coatings can correspond to nascent stages of glauconitization, which is favored under suboxic conditions in semi-enclosed skeletal pores or under thin sediment veneers (Bornhold and Giresse 1985; Odin and Fullagar 1988; Kelly and Webb 1999), is associated with dissolution of calcite and other minerals (Baldermann et al. 2012), and requires very slow sedimentation rates. Full transformation to glauconite at locations away from terrigenous sources requires residence times up to 10^5–10^6 years (Amorosi 2012; Baldermann et al. 2013; Baldermann et al. 2015). Alteration processes that occur at such slow rates have important implications for detecting very old cohorts in fossil assemblage because they provide minimum postmortem ages even when skeletal particles do not spend all time in the TAZ.

The bathyal habitats off New Caledonia provide conditions for formation of biostratigraphically condensed assemblages because (1) hemipelagic sedimentation rates in the center of the Loyalty Basin and to the south off New Caledonia at ~ 2,000 m are 1–3 cm/1000 years (Cotillon et al. 1989) and sedimentation rates on slopes determined by block-faulted morphology are dominated by erosion and sediment bypassing, and (2) nautiloid shells observed here co-occur with stratigraphically condensed assemblages of foraminifers that consist of a mixture of extant species and species that went extinct during the lower Pleistocene and during the mid-Pleistocene extinction event (Tomašových et al. 2016). However, the window of time averaging is not only determined by negligible or zero burial rates but also by disintegration rates. Nautiloid shells observed here apparently disintegrate at centennial scales (Tomašových et al. 2016), thus limiting the potential for a high contribution of very old shells to a death assemblage.

CONCLUSIONS

Some types of cephalopod damage can be used to distinguish among skeletal remains differing in postmortem age in comparable environments. Age-dated shells imply that massive degradation by boring sponges requires centuries to develop, and full discoloration and formation of clay-goethitic coatings and pore infills requires millennia to develop in the epibathyal zone, and centuries in the mesobathyal zone. Shells that are several centuries old possess right and left flanks significantly differing in preservation, and millennia-old specimens are represented by relict half-shells with only one flank preserved. Such asymmetric preservation and preservation of half-shells implies that shells were oriented horizontally in a more or less similar orientation on the sea-floor for a decades or even centuries. Bathyal environments off New Caledonia are thus weakly affected by the decoupling between postmortem age and preservation characteristic of shallow-water environments where reworking rate tends to be more frequent. We suggest that the strength of this relation is thus not only of interest for estimation of scales of time averaging but can also be informative for inferences about the rate of physical reworking or biological mixing in Holocene environments.

ACKNOWLEDGMENTS

We thank M. Reolid and an anonymous reviewer for comments, D. Marchand for introducing us to specimens collected by Biocal and Biogeocal cruises, J. Thomas and N. Landman for access to specimens deposited at the Université de Bourgogne and the American Museum of Natural History. We thank K. Zágoršek, B. Ekrt, and J. Kvaček (National Museum in Prague) for the access to the scanning electron microscope Hitachi S-3700N. This research was funded by the Slovak Scientific Grant Agency (VEGA 0136-15), the Slovak Agency for Research and Development (APVV 0644-10), and the European Regional Development Fund (ITMS-26220120064 and 26210120013).

REFERENCES

Albano, P.G., 2014, Comparison between death and living land mollusk assemblages in six forested habitats in northern Italy: PALAIOS, v. 29, p. 338–347.

Amorosi, A., 2012. The occurrence of glaucony in the stratigraphic record: distribution patterns and sequence-stratigraphic significance, *in* S. Morad, J.M. Ketzer, and L.F. De Ros (eds.), Linking Diagenesis to Sequence Stratigraphy: John Wiley and Sons, West Sussex, UK, p. 37–53.

Anderson, M.J. and Willis, T.J., 2003, Canonical analysis of principal coordinates: a useful method of constrained ordination for ecology: Ecology, v. 84, p. 511–525.

Baldermann, A., Grathoff, G.H., and Nickel, C., 2012, Micromilieu-controlled glauconitization in fecal pellets at Oker (Central Germany): Clay Minerals, v. 47, p. 513–538.

Baldermann, A., Warr, L.N., Grathoff, G.H., and Dietzel, M., 2013, The rate and mechanism of deep-sea glauconite formation at the Ivory Coast-Ghana marginal ridge: Clays and Clay Minerals, v. 61, p. 258–276.

Baldermann, A., Warr, L.N., Letofsky-Papst, I., and Mavromatis, V., 2015, Substantial iron sequestration during green-clay authigenesis in modern deep-sea sediments: Nature Geoscience, v. 8, p. 885–889.

Belanger, C.L., 2011, Evaluating taphonomic bias of paleoecological data in fossil benthic foraminiferal assemblages: PALAIOS, v. 26, p. 767–778.

Benito, M.I. and Reolid, M., 2012, Belemnite taphonomy (Upper Jurassic, Western Tethys) part II: fossil–diagenetic analysis including combined petrographic and geochemical techniques: Palaeogeography, Palaeoclimatology, Palaeoecology, v. 358, p. 89–108.

Bennington, J.B., 2003, Transcending patchiness in the comparative analysis of paleocommunities: a test case from the Upper Cretaceous of New Jersey: PALAIOS, v. 18, p. 22–33.

Best, M.M., 2008, Contrast in preservation of bivalve death assemblages in siliciclastic and carbonate tropical shelf settings: PALAIOS, v. 23, p. 796–809.

Bornhold, B.D. and Giresse, P., 1985, Glauconitic sediments on the continental shelf off Vancouver Island, British Columbia, Canada: Journal of Sedimentary Research, v. 55, p. 653–664.

Brayard, A., Escarguel, G., and Bucher, H., 2007, The biogeography of Early Triassic ammonoid faunas: clusters, gradients, and networks: Geobios, v. 40, p. 749–765.

Brühwiler, T., Bucher, H., Brayard, A., and Goudemand, N., 2010, High-resolution biochronology and diversity dynamics of the Early Triassic ammonoid recovery: the Smithian faunas of the Northern Indian Margin: Palaeogeography, Palaeoclimatology, Palaeoecology, v. 297, p. 491–501.

Calcinai, B., Bavestrello, G., and Cerrano, C., 2004, Bioerosion micro-patterns as diagnostic characteristics in boring sponges: Bollettino dei Musei e Degli Istituti Biologici dell'Università di Genova, v. 68, p. 229–238.

Calcinai, B., Cerrano, C., and Bavestrello, G., 2007, Three new species and one re-description of *Aka*: Journal of the Marine Biological Association of the United Kingdom, v. 87, p. 1355–1365.

Chamberlain, J.A., Jr., Ward, P.D., and Weaver, J.S., 1981, Post-mortem ascent of *Nautilus* shells: implications for cephalopod paleobiogeography: Paleobiology, v. 7, p. 494–509.

Chirat, R., 2000, The so-called "cosmopolitan" palaeogeographic distribution of Tertiary Nautilida of the genus *Aturia* Bronn 1838: the result of post-mortem transport by oceanic palaeocurrents: Palaeogeogeography, Palaeoclimatology, Palaeoecology, v. 157, p. 59–77.

Cichowolski, M., Pazos, P.J., Tunik, M.A., and Aguirre-Urreta, M.B., 2012, An exceptional storm accumulation of nautilids in the Lower Cretaceous of the Neuquén Basin, Argentina: Lethaia, v. 45, p. 121–138.

Cotillon, P., Liu, J.-D., Gaillard, C., and Evin, J., 1989, Evolution du taux de sedimentation au cours des derniers 30 000 ans aux abords de la Nouvelle-Caledonie (SW Pacifique): resultats de datations au radiocarbone et par la courbe de l'oxygene 18: Bulletin de la Societe Geologique de France, v. 5, p. 881–884, doi : 10.2113/gssgfbull.V.4.881.

De Forges, B.R., 1990, Les campagnes d'exploration de la faune bathyale dans la zone economique de la Nouvelle-Caledonie: Resultats des campagnes Musorstom, v. 6, p. 9–54.

Feely, R.A., Sabine, C.L., Lee, K., Millero, F.J., Lamb, M.F., Greeley, D., Bullister, J.L., Key, R.M., Peng, T.-H., Kozyr, A., Ono, T., and Wong, C.S., 2002, In situ calcium carbonate dissolution in the Pacific Ocean: Global Biogeochemical Cycles, v. 16, no. 1144, doi: 10.1029/2002GB001866.

Fernández-López, S.R., 2011, Taphonomic analysis and sequence stratigraphy of the *Albarracinites* beds (lower Bajocian, Iberian range, Spain), an example of shallow condensed section: Bulletin de la Société géologique de France, v. 182, p. 405–415.

Flessa, K.W., Cutler, A.H., and Meldahl, K.H., 1993, Time and taphonomy: quantitative estimates of time-averaging and stratigraphic disorder in a shallow marine habitat: Paleobiology, v. 19, p. 266–286.

Fürsich, F.T., 1978, The influence of faunal condensation and mixing on the preservation of fossil benthic communities: Lethaia, v. 11, p. 243–250.

Gagan, M.K., Hendy, E.J., Haberle, S.G., and Hantoro, W.S., 2004, Post-glacial evolution of the Indo-Pacific warm pool and El Niño-Southern Oscillation: Quaternary International, v. 118, p. 127–143.

Gerber, S., 2011, Comparing the differential filling of morphospace and allometric space through time: the morphological and developmental dynamics of Early Jurassic ammonoids: Paleobiology, v. 37, p. 369–382.

Gerhard, S. and Henrich, R., 2001, Shell preservation of *Limacina inflata* (Pteropoda) in surface sediments from the Central and South Atlantic Ocean: a new proxy to determine the aragonite saturation state of water masses: Deep-Sea Research I, v. 48, p. 2051–2071.

Goodwin, D.H., Flessa, K.W., Téllez-Duarte, M.A., Dettman, D.L., Schöne, B.R., and Avila-Serrano, G.A., 2004, Detecting time-averaging and spatial mixing using oxygen isotope variation: a case study: Palaeogeography, Palaeoclimatology, Palaeoecology, v. 205, p. 1–21.

Hassan, G.S., Tietze, E., Cristini, P.A., and De Francesco, C.G., 2014, Differential preservation of freshwater diatoms and mollusks in late Holocene sediments: paleoenvironmental implications. PALAIOS, v. 29, p. 612–623.

Hembree, D.I., Mapes, R.H., and Goiran, C., 2014, The impact of high-energy storms on shallow-water *Nautilus* (Cephalopoda) taphonomy, Lifou (Loyalty Islands): PALAIOS, v. 29, p. 348–362.

Jacobs, D.K., Landman, N.H., and Chamberlain, J.A., Jr., 1994, Ammonite shell shape covaries with facies and hydrodynamics: iterative evolution as a response to changes in basinal environment: Geology, v. 22, p. 905–908.

Kelly, J.C. and Webb, J.A., 1999, The genesis of glaucony in the Oligo-Miocene Torquay Group, southeastern Australia: petrographic and geochemical evidence: Sedimentary Geology, v. 125, p. 99–114.

Kidwell, S.M., 1989, Stratigraphic condensation of marine transgressive records: origin of major shell deposits in the Miocene of Maryland: Journal of Geology, v. 97, p. 1–24.

Kidwell, S.M., 1993, Patterns of time-averaging in the shallow marine fossil record, *in* S.M Kidwell and A.K. Behrensmeyer (eds.), Taphonomic Approaches to Time Resolution in Fossil Assemblages: Short Courses in Paleontology, The Paleontological Society, v. 6, p. 275–300.

Kidwell, S.M., 1998, Time-averaging in the marine fossil record: overview of strategies and uncertainties: Geobios, v. 30, p. 977–995.

Kidwell, S.M., 2013, Time-averaging and fidelity of modern death assemblages: building a taphonomic foundation for conservation palaeobiology: Palaeontology, v. 56, p. 487–522.

Kidwell, S.M., Best, M.M.R., and Kaufman, D., 2005, Taphonomic tradeoffs in tropical marine death assemblages: differential time-averaging, shell loss, and probable bias in siliciclastic versus carbonate facies: Geology, v. 33, p. 729–732.

Kidwell, S.M., Rothfus, T.A., and Best, M.M., 2001, Sensitivity of taphonomic signatures to sample size, sieve size, damage scoring system, and target taxa: PALAIOS, v. 16, p. 26–52.

Kim, S.-H. and Yi, S.V., 2007, Understanding relationship between sequence and functional evolution in yeast proteins: Genetica, v. 131, p. 151–156.

Kowalewski, M. and Bambach, R.K., 2003, The limits of paleontological resolution, *in* P.J Harries (ed.), Approaches in High-resolution Stratigraphic Paleontology: Kluwer, Boston, p. 1–48.

Kowalewski, M., Flessa, K.W., and Aggen, J.A., 1994, Taphofacies analysis of Recent shelly cheniers (beach ridges), northeastern Baja California, Mexico: Facies, v. 31, p. 209–241.

Kruta, I., Landman, N.H., and Cochran, J.K., 2014, A new approach for the determination of ammonite and nautilid habitats: PLOS One, v. 9, e87479.

Landman, N.H., Mapes, R.H., Cochran, J.K., Lignier, V., Hembree, D.I., Goiran, C., Folcher, E., and Brunet P., 2014, An unusual occurrence of *Nautilus macromphalus* in a cenote in the Loyalty Islands (New Caledonia): PLoS ONE, v. 9, e113372.

Lescinsky, H.L., Edinger, E., and Risk, M.J., 2002, Mollusc shell encrustation and bioerosion rates in a modern epeiric sea: taphonomy experiments in the Java Sea, Indonesia: PALAIOS, v. 17, p. 171–191.

Lukeneder, A. and Mayrhofer, S., 2014, Taphonomical implications from Upper Triassic mass flow deposits: 2-dimensional reconstructions of an ammonoid mass occurrence (Carnian, Taurus Mountains, Turkey): Geologica Carpathica, v. 65, p. 339–364.

Maeda, H., 1987, Taphonomy of ammonites from the Cretaceous Yezo Group in the Tappu area, northwestern Hokkaido, Japan: Transactions and Proceedings of the Palaeontological Society of Japan, New Series, v. 148, p. 285–305.

Maeda, H. and Seilacher, A., 1996, Ammonoid taphonomy, *in* N. Landman, K. Tanabe, and R.A. Davis (eds.), Ammonoid Paleobiology: Topics in Geobiology, v. 13, Plenum Press, New York, p. 543–578.

Mamo, B.L., Brock, G.A., and Gretton, E.J., 2013, Deep sea benthic foraminifera as proxies for palaeoclimatic fluctuations in the New Caledonia Basin, over the last 140,000 years: Marine Micropaleontology, v. 104, p. 1–13.

Mapes, R.H., Hembree, D.I., Rasor, B.A., Stigall, A., Goirand, C., and De Forges, B.R., 2010b, Modern *Nautilus* (Cephalopoda) taphonomy in a subtidal to backshore environment, Lifou (Loyalty Islands): PALAIOS, v. 25, p. 656–670.

Mapes, R.H., Landman, N.H., Cochran, K., Goiran, C., De Forges, B.R., and Renfro, A., 2010a, Early taphonomy and significance of naturally submerged *Nautilus* shells from the New Caledonia region: PALAIOS, v. 25, p. 597–610.

Mapes, R.H. and Larson, N.L., 2015, Ammonoid Color Patterns, *in* C. Klug, D. Korn, K. De Baets, I. Kruta, and R.H. Mapes (eds.), Ammonoid Paleobiology: From Anatomy to Ecology: Springer, Dordrecht, p. 25–44.

Martire, L., 1992, Sequence stratigraphy and condensed pelagic sediments, an example from the Rosso Ammonitico Veronese, northeastern Italy: Palaeogeography, Palaeoclimatology, Palaeoecology, v. 94, p. 169–191.

Meldahl, K.H. and Flessa, K.W., 1990, Taphonomic pathways and comparative biofacies and taphofacies in a Recent intertidal/shallow shelf environment: Lethaia, v. 23, p. 43–60.

Meldahl, K.H., Flessa, K.W., and Cutler, A.H., 1997, Time-averaging and postmortem skeletal survival in benthic fossil assemblages: quantitative comparisons among Holocene environments: Paleobiology, v. 23, p. 207–229.

Middelburg, J.J., Soetaert, K., and Herman, P.M.J., 1997, Empirical relationships for use in global diagenetic models: Deep-Sea Research I, v. 44, p. 327–344.

Miller, J.H., Behrensmeyer, A.K., Du, A., Lyons, S.K., Patterson, D., Tóth, A., Villaseñor, A., Kanga, E., and Reed, D., 2014, Ecological fidelity of functional traits based on species presence-absence in a modern mammalian bone assemblage (Amboseli, Kenya): Paleobiology, v. 40, p. 560–583.

Naglik, C., Rikhtegar, F., and Klug, C., 2016, Buoyancy of some Palaeozoic ammonoids and their hydrostatic properties based on empirical 3D-models: Lethaia, v. 49, p. 3–12.

Nelson, C.S. and Bornhold, B.D., 1983, Temperate skeletal carbonate sediments on Scott shelf, northwestern Vancouver Island, Canada: Marine Geology, v. 52, p. 241–266.

Nieto, L.M., Reolid, M., Molina, J.M., Ruiz-Ortiz, P.A., Jiménez-Millán, J., and Rey, J., 2012, Evolution of pelagic swells from hardground analysis (Bathonian–Oxfordian, Eastern External Subbetic, southern Spain): Facies, v. 58, p. 389–414.

Nieto, L.M., Ruiz-Ortiz, P.A., Rey, J. and Benito, M.I., 2008, Strontium-isotope stratigraphy as a constraint on the age of condensed levels: examples from the Jurassic of the Subbetic Zone (southern Spain): Sedimentology, v. 55, p. 1–29.

Norris, R.M. and Grant-Taylor, T.L., 1989, Late Quaternary shellbeds, western shelf, New Zealand: New Zealand Journal of Geology and Geophysics, v. 32, p. 343–356.

Oda, H., Usui, A., Miyagi, I., Joshima, M., Weiss, B.P., Shantz, C., Fong, L.E., McBride, K.K., Harder, R., and Baudenbacher, F.J., 2011, Ultrafine-scale magnetostratigraphy of marine ferromanganese crust: Geology, v. 39, p. 227–230.

Odin, G.S. and Fullagar, P.D., 1988, Geological significance of the glaucony facies, *in* G.S. Odin (ed.), Green Marine Clays: Elsevier, Amsterdam, p. 295–332.

Oksanen, J., Blanchet, F.G., Kindt, R., Legendre, P., Minchin, P.R., O'Hara, R.B., Simpson, G.L., Solymos, P., Stevens, M.H.H., and Wagner, H., 2015, Vegan: community ecology package: http://CRAN.R-project.org/package=vegan.

Olóriz, F., Reolid, M., and Rodríguez-Tovar, F.J., 2002, Fossil assemblages, lithofacies, taphofacies and interpreting depositional dynamics in the epicontinental Oxfordian of the Prebetic Zone, Betic Cordillera, southern Spain: Palaeogeography, Palaeoclimatology, Palaeoecology, v. 185, p. 53–75.

Olóriz, F., Reolid, M., and Rodríguez-Tovar, F.J., 2004, Taphonomy of ammonite assemblages from the middle-upper Oxfordian (Transversarium?-Bifurcatus Zones) in the Internal Prebetic (Betic Cordillera, southern Spain): taphonic populations and taphofacies to support ecostratigraphic interpretations: Rivista Italiana di Paleontologia e Stratigrafia, v. 110, p. 239–248.

Olóriz, F., Reolid, M., and Rodríguez-Tovar, F.J., 2006, Approaching trophic structure in Late Jurassic neritic shelves: a western Tethys example from southern Iberia: Earth-Science Reviews, v. 79, p. 101–139.

Olszewski, T.D., 2004, Modeling the influence of taphonomic destruction, reworking, and burial on time-averaging in fossil accumulations: PALAIOS, v. 19, p. 39–50.

Parsons-Hubbard, K., 2005, Molluscan taphofacies in recent carbonate reef/lagoon systems and their application to sub-fossil samples from reef cores: PALAIOS, v. 20, p. 175–191.

Pilkey, O.H., Fierman, E.I., and Trumbull, J.V.A., 1979, Relationship between physical condition of the carbonate fraction and sediment environments: northern Puerto Rico shelf: Sedimentary Geology, v. 24, p. 283–290.

Powell, E.N., Brett, C.E., Parsons-Hubbard, K.M., Callender, W.R., Staff, G.M., Walker, S.E., Raymond, A., and Ashton-Alcox, K.A., 2011, The relationship of bionts and taphonomic processes in molluscan taphofacies formation on the continental shelf and slope: eight-year trends: Gulf of Mexico and Bahamas: Facies, v. 57, p. 15–37.

Powell, E.N. and Davies, D.J., 1990, When is an 'old' shell really old?: Journal of Geology, v. 98, p. 823–844.

Powell, E.N., Hu, X., Cai, W.-J., Ashton-Alcox, K.A., Parsons-Hubbard, K.M., and Walker, S.E., 2012, Geochemical controls on carbonate shell taphonomy in Northern Gulf of Mexico continental shelf and slope sediments: PALAIOS, v. 27, p. 571–584.

Reolid, M., Nieto, L.M., and Rey, J., 2010, Taphonomy of cephalopod assemblages from Middle Jurassic hardgrounds of pelagic swells (South-Iberian Palaeomargin, Western Tethys): Palaeogeography, Palaeoclimatology, Palaeoecology, v. 292, p. 257–271.

Reyment, R.A., 1973, Factors in the distribution of fossil cephalopods, part 3, experiments with exact models of certain shell type: Bulletin of the Geological Institutions of the University of Uppsala, N.S., v. 4, p. 7–41.

Richardson-White, S. and Walker, S.E., 2011, Diversity, taphonomy and behavior of encrusting foraminifera on experimental shells deployed along a shelf-to-slope bathymetric gradient, Lee Stocking Island, Bahamas: Palaeogeography, Palaeoclimatology, Palaeoecology, v. 312, p. 305–324.

Ritter, M., Erthal, F., and Coimbra, J.C., 2013, Taphonomic signatures in molluscan fossil assemblages from the Holocene lagoon system in the northern part of the coastal plain, Rio Grande do Sul State, Brazil: Quaternary International, v. 305, p. 5–14.

Rivers, J.M., James, N.P., Kyser, T.K., and Bone, Y., 2007, Genesis of palimpsest cool-water carbonate sediment on the continental margin of southern Australia: Journal of Sedimentary Research, v. 77, p. 480–494.

Roux, M., 1994, The CALSUB cruise on the bathyal slopes off New Caledonia: Mémoires du Muséum national d'Histoire naturelle, v. 161, p. 9–47.

Roux, M., Bouchet, P., Bourseau, J.-P., Gaillard, C., Grandperrin, R., Guille, A., Laurin, B., Monniot, C., De Forges, B.R., Rio, M., Segonzac, M., Vacelet, J. and Zibrowius, H., 1991, L'environnement bathyal au large de la Nouvelle-Calédonie: résultats préliminaires de la campagne CALSUB et conséquences paléoécologiques: Bulletin de la Société Géologique de France, v. 162, p. 675–685.

Santantonio, M., 1993, Facies associations and evolution of pelagic carbonate platform/basin systems: examples from the Italian Jurassic: Sedimentology, v. 40, p. 1039–1067.

Scarponi, D., Kaufman, D., Amorosi, A., and Kowalewski, M., 2013, Sequence stratigraphy and the resolution of the fossil record: Geology, v. 41, p. 239–242.

Seilacher, A., Andalib, F., Dietl, G., and Gocht, H., 1976, Preservational history of compressed Jurassic ammonites from Southern Germany: Neues Jahrbuch für Geologie und Paläontologie, Abhandlungen, v. 152, p. 303–356.

Seuss, B., Hembree, D.I., Wisshak, M., Mapes, R.H., and Landman, N.H., 2015b, Taphonomy of backshore versus deep–marine collected *Nautilus macromphalus* conchs (New Caledonia): PALAIOS, v. 30, p. 503–513.

Seuss, B., Wisshak, M., Mapes, R.H., and Landman, N.H., 2015a, Syn-vivo bioerosion of *Nautilus* by endo- and epilithic foraminiferans (New Caledonia and Vanuatu): PLoS ONE, v. 10, e0125558.

Tanabe, K., Inazumi, A., Tamahama, K., and Katsuta, T., 1984, Taphonomy of half and compressed ammonites from the Lower Jurassic black shales of the Toyora area, west Japan: Palaeogeography, Palaeoclimatology, Palaeoecology, v. 47, p. 329–346.

Terry, R.C. and Novak, M., 2015, Where does the time go?: mixing and the depth-dependent distribution of fossil ages: Geology, v. 43, p. 487–490.

Tomašových, A., Fürsich, F.T., and Olszewski, T.D., 2006, Modeling shelliness and alteration in shell beds: variation in hardpart-input and burial rates leads to opposing predictions: Paleobiology, v. 32, p. 278–298.

Tomašových A. and Kidwell, S.M., 2010, Predicting the effects of increasing temporal scale on species composition, diversity, and rank-abundance distributions: Paleobiology, v. 36, p. 672–695.

Tomašových, A., Kidwell, S.M., Foygel Barber, R., and Kaufman, D.S., 2014, Long-term accumulation of carbonate shells reflects a 100-fold drop in loss rate: Geology, v. 42, p. 819–822.

Tomašových, A. and Schlögl, J., 2008, Analyzing variations in cephalopod abundances in shell concentrations: the combined effects of production and density-dependent cementation rates: PALAIOS, v. 23, p. 648–666.

Tomašových, A., Schlögl, J., Kaufman, D.S., and Hudáčková, N., 2016, Temporal and bathymetric resolution of nautiloid death assemblages in stratigraphically condensed oozes (New Caledonia): Terra Nova, v. 28, p. 271–278.

Torres, T., Ortiz, J.E., and Arribas, I., 2013, Variations in racemization/epimerization ratios and amino acid content of *Glycymeris* shells in raised marine deposits in the Mediterranean: Quaternary Geochronology, v. 16, p. 35–49.

Trauth, M.H., Sarnthein, M., and Arnold, M., 1997, Bioturbational mixing depth and carbon flux at the seafloor: Paleoceanography, v. 12, p. 517–526.

Wani, R., 2001, Reworked ammonoids and their taphonomic implications in the Upper Cretaceous of northwestern Hokkaido, Japan: Cretaceous Research, v. 22, p. 615–625.

Wani, R., 2004, Experimental fragmentation patterns of modern *Nautilus* shells and the implications for fossil cephalopod taphonomy: Lethaia, v. 37, p. 113–123.

Wani, R. and Ikeda, H., 2006, Planispiral cephalopod shells as a sensitive indicator of modern and ancient bottom currents: new data from flow experiments with modern *Nautilus pompilius*: PALAIOS, v. 21, p. 289–297.

Wani, R., Kase, T., Shigeta, Y., and De Ocampo, R., 2005, New look at ammonoid taphonomy, based on field experiments with modern chambered nautilus: Geology, v. 33, p. 849–852.

Weedon, G.P., Jenkyns, H.C., Coe, A.L., and Hesselbo, S.P., 1999, Astronomical calibration of the Jurassic time-scale from cyclostratigraphy in British mudrock formations: Philosophical Transactions of the Royal Society of London A: Mathematical, Physical and Engineering Sciences, v. 357, p. 1787–1813.

Wehmiller, J.F., York, L.L., and Bart, M.L., 1995, Amino acid racemization geochronology of reworked Quaternary mollusks on U.S. Atlantic coast beaches: implications for chronostratigraphy, taphonomy, and coastal sediment transport: Marine Geology, v. 124, p. 303–337.

Wilson, J.B., 1988, A model for temporal changes in the faunal composition of shell gravels during a transgression on the continental shelf around the British Isles: Sedimentary Geology, v. 60, p. 95–105.

Wisshak, M., Tribollet, A., Golubic, S., Jakobsen, J., and Freiwald, A., 2011, Temperate bioerosion: ichnodiversity and biodiversity from intertidal to bathyal depths (Azores): Geobiology, v. 9, p. 492–520.

Wisshak, M., Berning, B., Jakobsen, J., and Freiwald, A., 2015, Temperate carbonate production: biodiversity of calcareous epiliths from intertidal to bathyal depths (Azores): Marine Biodiversity, v. 45, p. 87–112.

Yanes, Y., 2012, Shell taphonomy and fidelity of living, dead, Holocene, and Pleistocene land snail assemblages: PALAIOS, 27, p. 127–136.

Zuschin, M. and Stanton, R.J., 2002, Paleocommunity reconstruction from shell beds: a case study from the Main Glauconite Bed, Eocene, Texas: PALAIOS, v. 17, p. 602–614.

Received 22 March 2016; accepted 9 November 2016.